XSPECT
Observer's Handbook

Preliminary version 0.4, 12 June 1997

Edited by Kristian Pedersen & Jamila Oukbir

Danish Space Research Institute
Juliane Maries Vej 30
2100 København Ø
Denmark

Contents

List of Figures

List of Tables

Preface

This is the first version of an Observer's Handbook – aimed at the potential XSPECT observers. This Handbook can also be found as a postscript document at the DSRI home–page: http://www.dsri.dk/srg/userman.ps.

The idea is to present the main characteristics of the XSPECT instruments and to give the current best estimates of XSPECT's capabilities. The technicalities have been kept at a rather low level, only brief presentations of the instruments are given. More details can be found in the papers in the reference list. At the time of writing some issues still need to be settled, but they should be resolved during Summer 1997.

Only instruments build by DSRI are described in this Handbook. For descriptions of all the SRG instruments, see the list of other sources of information at the back. A list of contact persons for various matters is also given given at the back.

Readers familiar with the XSPECT instruments can go directly to the chapter "Feasibility of observations and observation planning" for a discussion of observational issues.

Proposal handling is not described in this Handbook, for details we refer to the DSRI home–page: http://www.dsri.dk.

This Handbook has been edited by us, but a number of people has contributed significantly to all parts: Finn E. Christensen, Carl Budtz–Jørgensen, Mattias Møhl Madsen, Niels Jørgen Westergaard, Allan Hornstrup, Bent Madsen (all from DSRI, Copenhagen) and Hans Wiebicke, Ingolf Halm (AIP, Germany). Furthermore, parts of this Handbook have been taken from a draft to a similar Handbook made by the US SRG Coordination Facility.

Kristian Pedersen & Jamila Oukbir, 12/6 1997.

Spectrum–Røntgen–Gamma overview

Observing platform

Spectrum–Røntgen–Gamma (SRG) is an observatory being developed under the sponsorship of the Russian Academy of Sciences, with instruments contributed by numerous European countries and the US. The major facility on SRG is SODART (Soviet–Danish Röntgen Telescope). This system consists of twin, thin–foil, conical X–ray telescopes (hereafter called FM1 and FM2) developed by DSRI and focal plane instruments which are briefly described in the next section. In addition, there are also a set of UV telescopes, TAUVEX, which are co–aligned with SODART. A sketch of SRG is shown on Fig. (2.1) with all the other instruments flying aboard the satellite (JET–X, MART–LIME, MOXE, FUVITA, SPIN).

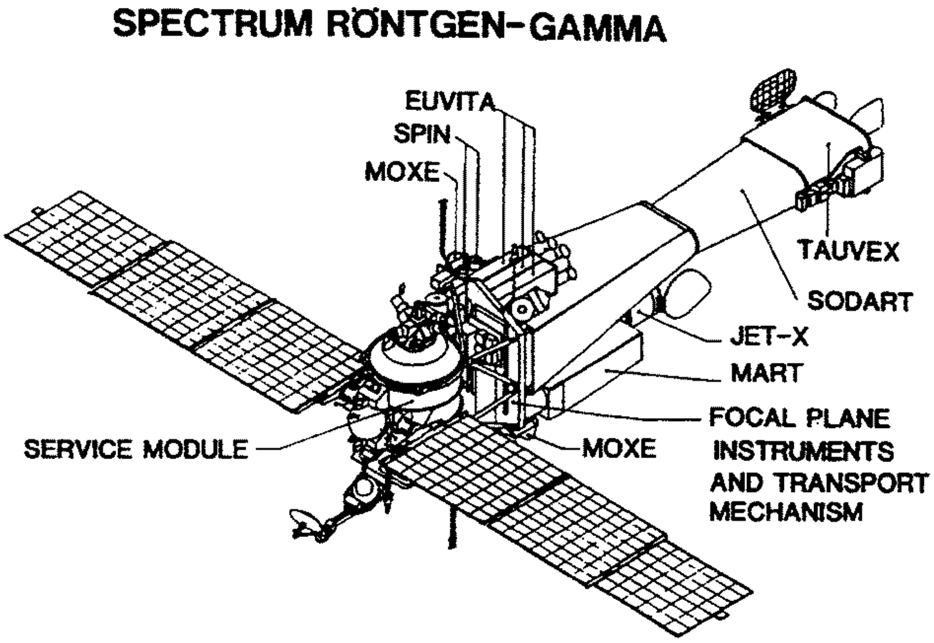

Figure 2.1: Spectrum–Røntgen–Gamma instrumentation. From Schnopper (1994).

List of instruments

A slide in each focal plane makes the exchange of focal plane instruments possible. The focal plane instruments that may be selected with FM1 are:

- Low Energy (0.2 – 8 keV) Proportional Counter (LEPC–1), an imaging proportional counter with 13% energy resolution at 6 keV and ~ 1 mm position resolution, developed by DSRI.
- High Energy (2 – 25 keV) Proportional Counter (HEPC–1) with properties similar to the LEPC, also developed by DSRI.
- Silicon X–ray Array (SIXA), an array of solid state detectors for moderate resolution spectroscopy from 0.5 – 20 keV, developed by the University of Helsinki and the Russian Space Research Institute (IKI).
- Focal Plane X–ray Detector (FRD–A), a high energy (2 – 25 keV) imaging proportional counter similar to HEPC developed by IKI.

The focal plane instruments that may be selected with FM2 are:

- LEPC–2, HEPC–2 and FRD–2 (duplicates of LEPC–1, HEPC–1 and FRD–A1).
- X–ray Polarimeter (SXRP), developed by Columbia University.
- Objective Crystal Spectrometer (OCS), allowing high energy spectroscopy ($\Delta E/E \sim 100 - 1000$ in four energy ranges: 0.20 – 0.285 keV, 0.60 – 1.2 keV, 2.50 – 5.0 keV and 5.0 – 10.0 keV. OCS is developed by DSRI, the Max–Planck–Institut and IKI.

The SODART system with all the telescopes and instruments is represented in Fig. (2.2). In the following, only the instruments developed by DSRI will be described. Informations concerning SIXA can be found in Vilhu et al. (1994).

Orbit and pointing accuracy

Spectrum–Røntgen–Gamma will be launched into a deep highly eccentric orbit with a period of about four days. This choice of orbit enables long duration, up to about 80h observations to be made. Ground station operations which include up and down–links for data and command transfer will take place every 18 to 30 hours. As experience grows, it should be possible to plan for at least 10 reorientations of the spacecraft per 24 hour period. With all the operational and pointing constraints (see below) taken into account, there will be access to approximately 80% of the celestial sphere at any time (cf. next section).

The spacecraft pointing is controlled by a Sun sensor which stabilizes one axis and two star sensors, one of which stabilizes a second axis, However, the pointing stabilisation has not been finally settled. The star sensors use only a small set (~ 15) bright stars which has the consequence of restricting the allowed viewing direction. The SRG Observatory pointing system provides absolute pointing accuracy to 2 arcminutes in each coordinate (at a probability level of 90%). However, using a feed back system from TAUVEX the absolute pointing accuracy may be $3''$, but this is still under consideration. The settling time after a slew is at most 5 minutes. The pointing stability is better than 5 arcseconds

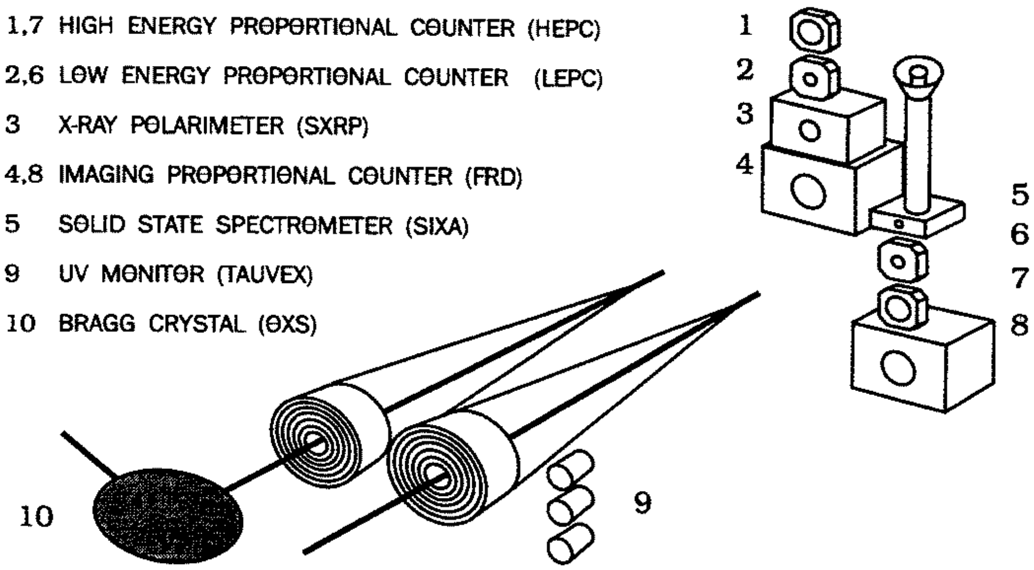

Figure 2.2: The SODART system: Telescopes and instruments. From Schnopper (1994).

over a one minute interval with a limit cycle of 30 arcseconds from the nominal attitude. The maximum drift rate is 1.0×10^{-4} arcseconds per second during pointing mode and the slew rate is at least 0.35 degrees per second. The post–facto aspect reconstruction will be 35 arcseconds or better for the spacecraft. Additional aspect information will be provided by the TAUVEX UV telescope which is co–aligned with SODART and mounted to the SODART tube. The details of the aspect solution to be provided by TAUVEX are not yet specified.

Viewing constraints

The orientation of the Spectrum-X-Gamma platform is constrained by several factors. If one defines the telescope pointing direction as the X axis and the solar panel pointing direction as the $-Z$ axis, then the Sun must be within 10° of the XZ plane and within 40° of the YZ plane. Further, the two star sensors, which can only use stars brighter than about magnitude 1.0, view in planes 20° from XY plane towards $-Z$, and between 70° and 140° from the X axis. These constraints are illustrated in Fig. (2.3) (The star sensor positions are not clear on the figure).

Subject to the above viewing constraints and the orbit of SRG, there will be a region on the sky never accesible to SRT. This "blind spot" will be about 30° by 30°, changing a bit with the evolution of the SRG orbit. The "blind spot" is situated approximately in the belt between $\delta = -10^\circ$ to $\delta = -40^\circ$ and depending on the launch parameters it can be placed at any right ascension.

When the OCS instrument is operating, the X–axis is constrained to view along an arc 90° from the OCS target and between 50° and 130° from the Sun. The precise location of the arc depends on the Sun position, as is shown in Fig. (2.4). In ecliptic coordinates the Sun is in the horizontal plane, and the OCS can view a point at ecliptic latitude lat. when the Sun is between S1 and S2, and again 6 months later. As the Sun direction

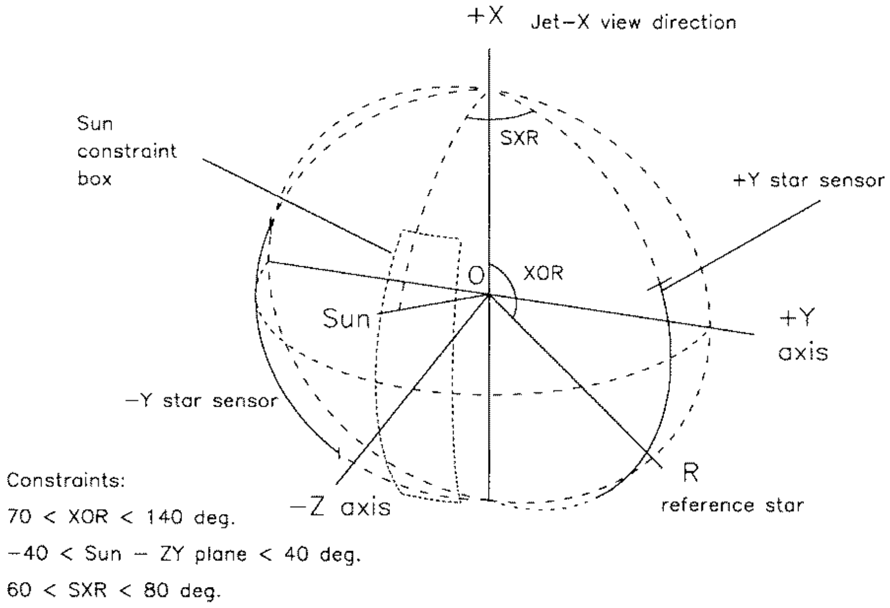

Figure 2.3: Guide star and Sun constraints on SRG viewing direction. Courtesy US SRG Coordination Facility.

changes from S1 to S2, the arc the telescope can view changes; the total accessible arc is approximately $80^\circ + 20$ Sin(lat.).The OCS can view the ecliptic pole at any time, and the telescope can view any point in the ecliptic plane if the date is chosen appropriately. The above is, of course, subject to a star being available for the star sensor in a suitable position.

This description is taken from the User's Manual for JMAN, a program for determining viewing opportunities for the JET-X instrument (M. Ricketts, Rutherford Appleton Laboratory, JET-X(93)RAL-150.1). Since the Jet-X and SODART telescopes are co-aligned, it is generally applicable to the SODART instruments as well.

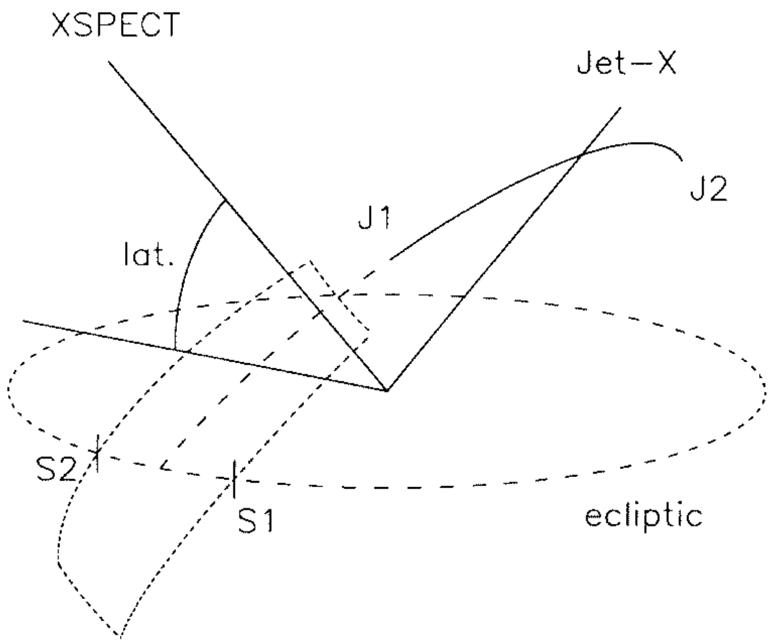

Figure 2.4: OCS viewing constraints. Courtesy US SRG Coordination Facility.

Mirror system

Introduction

The SODART mirror system consists of two high throughput X–ray telescopes. Each telescope is a highly nested conical approximation to a Wolter 1 geometry (see Fig. (3.1)). The mirrors are Au–coated and diplacquered Al foils which are rolled into a cylindrical shape and precisely mounted in two conical sections. A telescope is divided into four quadrants and each quadrant, consisting of two conical sections, is assembled and adjusted before assembly into a complete telescope. The telescopes have been designed to yield the highest effective area (the effective area is the "effective" collecting area) above 8 keV of any currently planned X–ray telescopes. Table 3.1 gives few parameters concerning the SODART telescope.

Six thousand individual mirrors have been produced by DSRI. Detailed optical measurement program of these mirrors have allowed the selection of the best 50% in order to be mounted in the flight telescope and the spare telescope. A very precise mounting of the mirrors near the edges of the quadrants as well as an accurate procedure for adjusting the spokes which position the mirrors in the radial direction in each quadrant enabled to built two flight telescopes having good imaging capabilities. Fig. (3.2) is a picture of one of the SODART mirror modules. The imaging properties are reflected in Fig. (3.3) which shows the on–axis image of a point source at 6.627 keV. From this figure it can be noticed that the quadrant structure of the telescope is obvious. The imaging efficiency of the two flight telescopes has already been tested and the results are presented in the next two sections. More details can be found in Christensen et al. (1997).

Focal length	8000 mm
Outer radius	300 mm
Inner radius	81.6 mm
Grazing angle range	0.147–0.535 deg
Number of mirrors	143
Reflecting surface	35 nm Au
Mirror thickness	0.4 mm
Mirror length for one section	200mm
Weight per telescope	101 kg

Table 3.1: SODART telescope parameters.

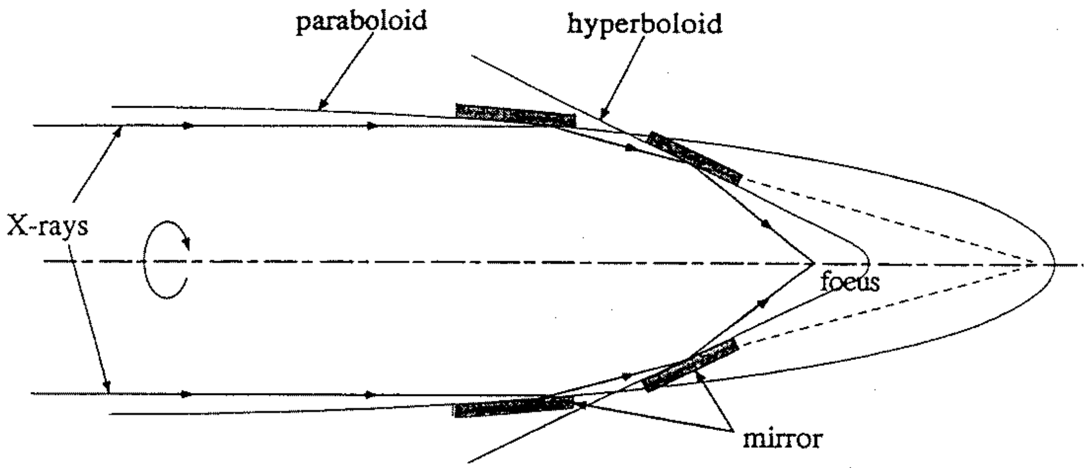

Figure 3.1: Conical appromixation to a Wolter I optics employed for SODART. From Ishisaki (1996).

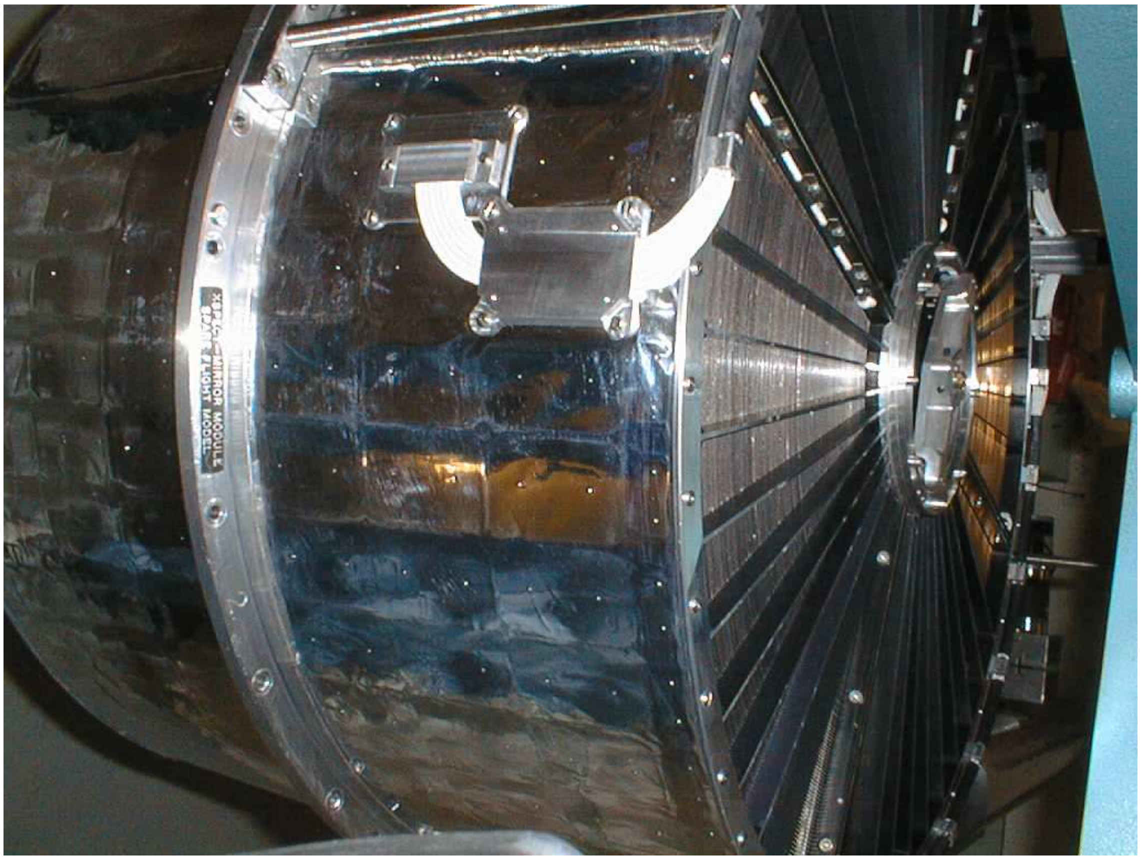

Figure 3.2: Picture of the SODART mirror module.

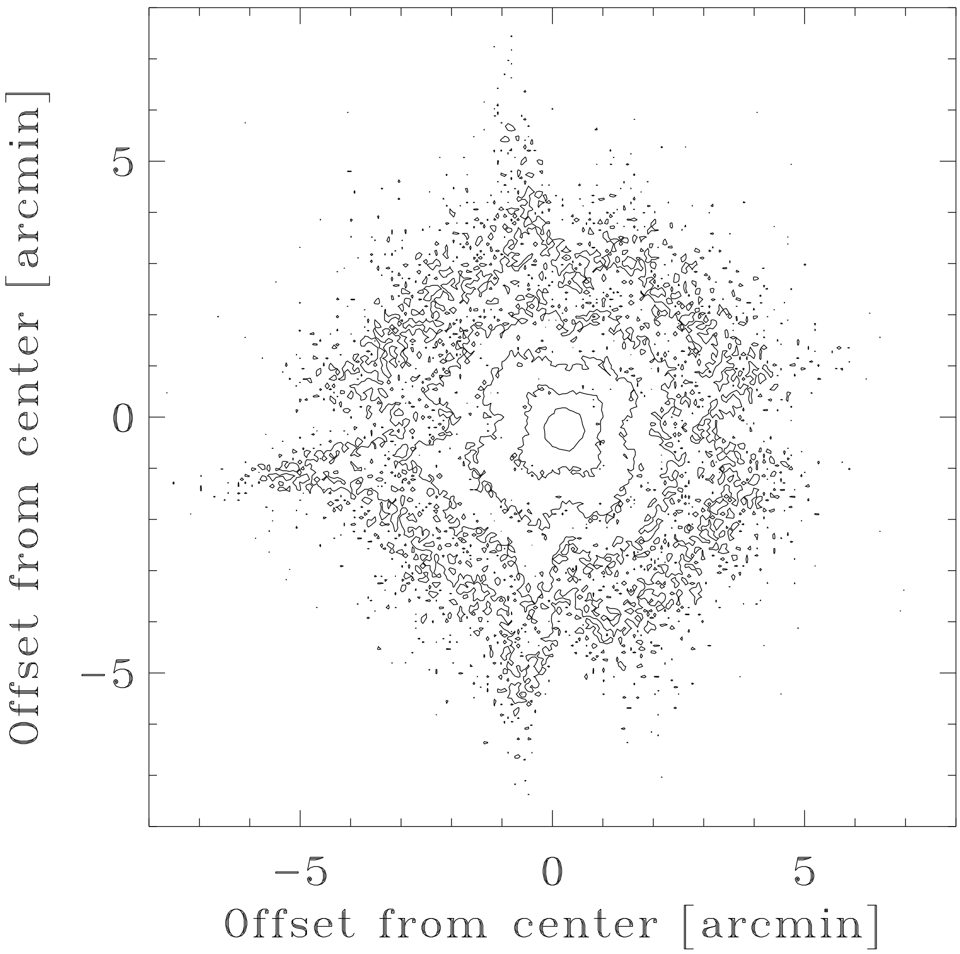

Figure 3.3: On–axis image at 6.627 keV for FM1. The x and y axis are offsets from the image center in arcmin. The data was recorded in a two–dimensional detector, similar to LEPC. There is a factor of 2.7183 between contours.

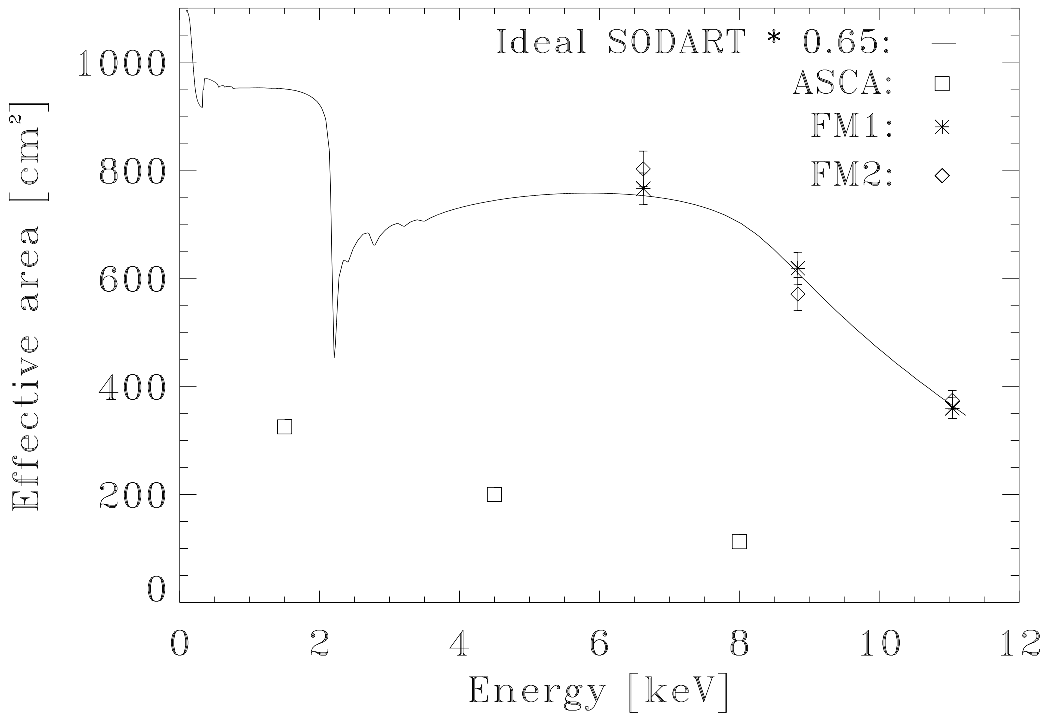

Figure 3.4: Measured on–axis effective area for FM1 and FM2 compared to the measured on–axis effective area for one ASCA telescope and 65% of the calculated ideal SODART area. The FOV for the FM1 and FM2 data is 105 arcmin. The FOV for the ASCA data is 12 arcmin.

Mirror Effective area and vignetting

Fig. (3.4) shows the measured on–axis effective area for the two flight telescopes (hereafter FM1 and FM2) at 6.627 keV, 8.837 keV and 11.046 keV. The data have been integrated over a FOV of 105 arcmin. The full line in this figure represent 65% of the predicted on–axis effective area from an ideal SODART telescope. Also represented in this figure the measured on–axis effective area at 1.5 keV, 4.5 keV and 8.0 keV for one ASCA telescope integrated over a FOV of 12 arcmin. It is of interest to notice that the measured on–axis effective area of ASCA also present an approximate 35% loss compared to its ideal geometry predictions.

The off-axis effective area for both telescopes has also been recorded at 6.627 keV, 8.837 keV and 11.046 keV, and the results are presented in Fig. (3.5). The points represent relative off-axis responses at different positions.

Encircled energy and point spread function

The encircled energy is the integrated intensity versus the image radius normalized with the total intensity in the image. Fig. (3.6) shows the encircled energy data for FM1 at 6.627 keV, 8.837 keV and 11.046 keV, measured within a FOV of 105 arcmin. From this figure, we can see that the imaging performance improves slightly with increasing

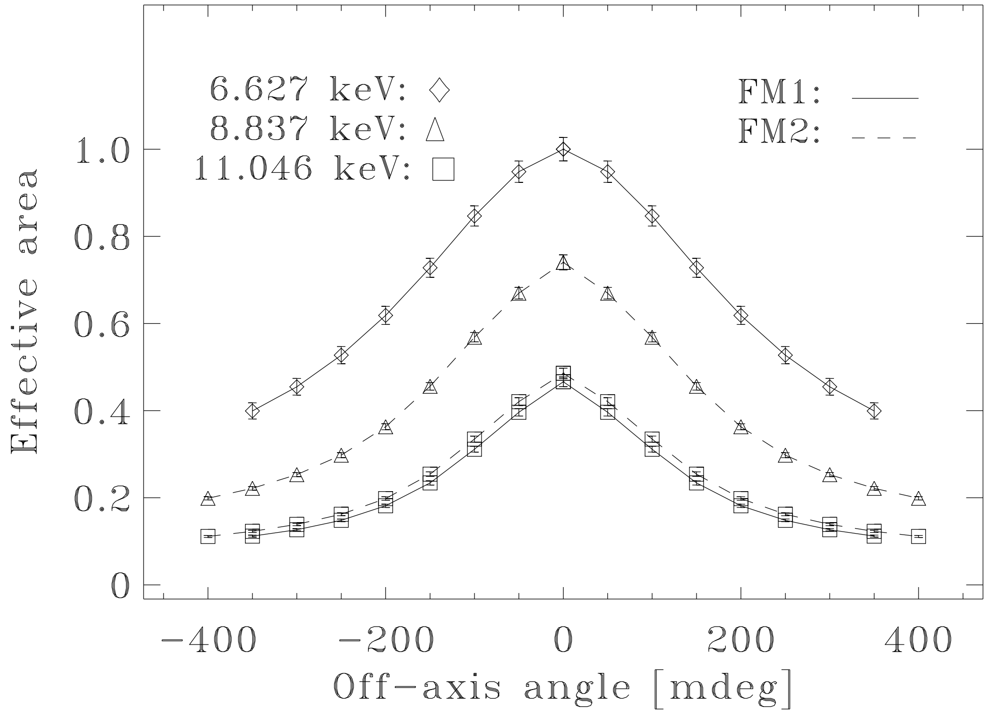

Figure 3.5: The measured off–axis effective area for FM1 and FM2. The lines are guide for the eye only.

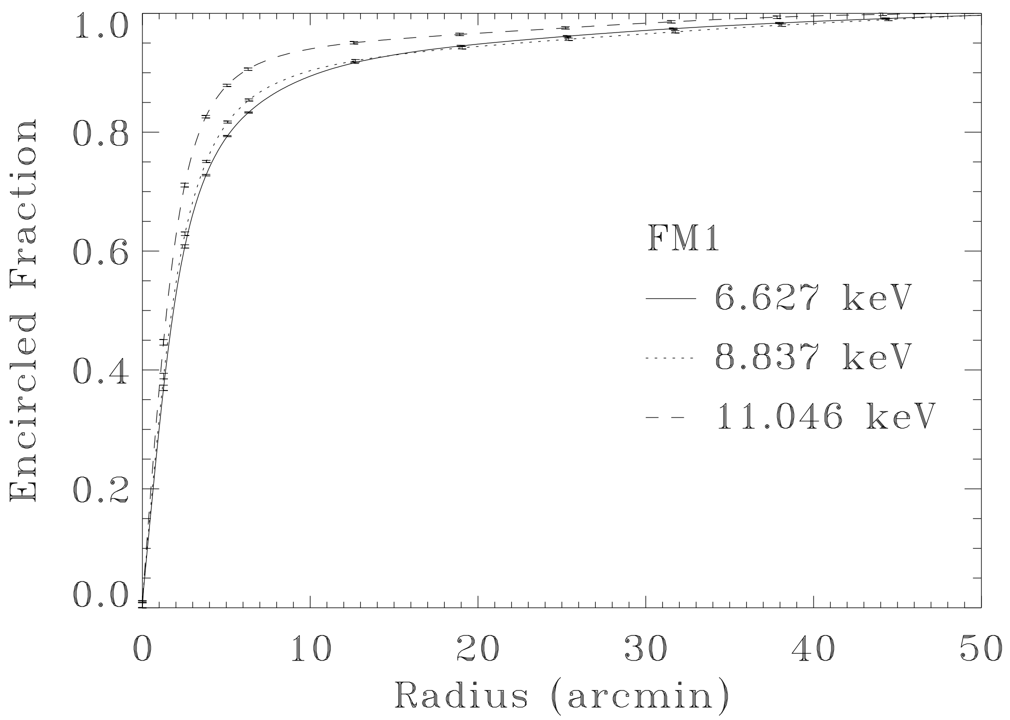

Figure 3.6: On–axis encircled energy for FM1 at 6.627 keV, 8.837 keV and 11.046 keV.

energy. This is due to the overall poorer figure of the outermost mirrors which becomes increasingly ineffective as the energy is increased.

The point spread function is the intensity distribution as a function of the distance from the image center. Fig. (3.7) shows the PSF at 6.627 keV for FM1, measured under the same conditions as the encircled energy. A simple functional representation of the PSF is given by the sum of a Gaussian divided by the radius and two exponential terms:

$$f(r) = (a_1/r)\exp(-0.5(r/b_1))^2 + a2\exp(-r/b_2) + a3\exp(-r/b_3).$$

The parameters of this function are $a1 = 0.01732$ arcmin, $a2 = 0.0024$, $a3 = 3.047 \times 10^{-5}$, $b1 = 1.835$ arcmin, $b2 = 2.659$ arcmin and $b3 = 14.559$ arcmin. The above function can be equally well used for the fitting of the PSF for all three energies with a slight variation of the parameters. The value of these parameters can be obtained upon request to Finn E. Christensen (DSRI) at **finn@dsri.dk**.

The off–axis PSF was also measured and in the next issue of this Handbook the corresponding data will be included. In addition, in flight calibrations will provide the PSF as a function of energy and position in the FOV. This will be achieved by many pointings of known bright point sources.

Ghost rays

Normally, X–ray photons reach the focal plane after reflection by both the primary and secondary mirrors. However, it is possible for singly reflected rays, or rays for which one

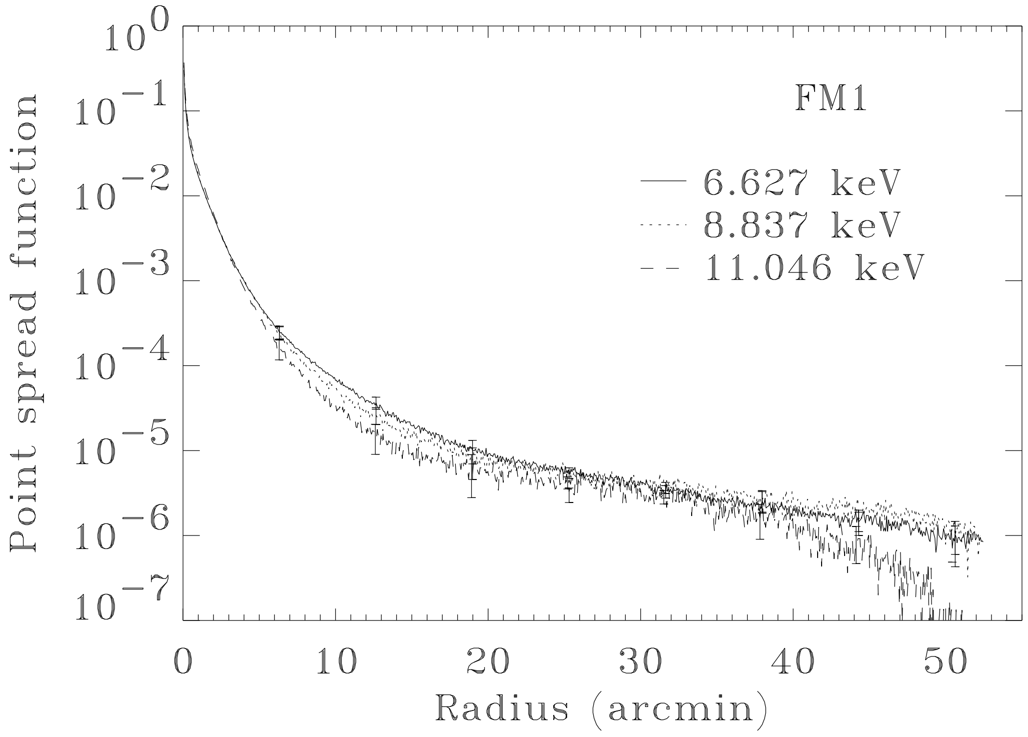

Figure 3.7: On–axis point spread function for FM1 at 6.627 keV, 8.837 keV and 11.046 keV.

of the two reflections involves the back of a mirror, to reach the focal plane. Any photons reaching the focal plane without undergoing the nominal sequence of two successive reflections from the front surface of the two X–ray telescopes constitute stray light. These photons are not properly imaged and form a quasi diffuse background. Considering stray light is very important whenever one observes a weak source near a source strong enough to contaminate the field of view. Ray–tracing simulations are currently under way (Westergaard et al.) in order to reproduce the effects of stray light and in–flight calibrations will also provide informations concerning the patterns of these rays.

The LEPC and HEPC detectors

Design principles and method of operations

For each of the telescopes a High Energy Proportional Counter (HEPC) and Low Energy Proportional Counter (LEPC) can be placed in the focal plane. The detectors employ the novel micro strip gas counter technology where the wire grids of the conventional proportional counters are replaced by a narrowly spaced conducting micro strips accurately deposited on an insulating substrate and a position sensing wire grid located perpendicular to and 1 mm above the micro strip plate. The electric field distribution allows electrons to drift past the wire grid to reach the anode strips where an avalanche is formed. The wire grid and the micro strips of a HEPC detector is shown in Fig. (4.1).

The LEPC and the HEPC micro strip plates are built into identical detector boxes made of Titanium, closed with X–ray windows and containing the counter gas, 90% Xe and 10% Methane. One LEPC and one HEPC is mounted together sharing a common gas reservoir. Both detectors tolerate a gas gain up to about 10^4 enabling detection of photons down to about 200 eV (for the LEPC) and to maintain an adequate image quality. The energy resolution is at least as good as conventional proportional counters.

For more extensive descriptions of LEPC and HEPC, see Budtz–Jørgensen et al. (1992); Budtz–Jørgensen et al. (1990); Budtz–Jørgensen et al. (1994a); Budtz–Jørgensen et al. (1994b). In the following, all statements apply to LEPC as well to HEPC unless explicitly stated.

LEPC specific matters

The LEPC micro strip plate is quadratic and the sensitive area measures 82 mm by 82 mm, see Fig. (4.2). The entrance window is circular with a diameter of 70 mm yielding a circular field of view (FOV) with diameter 30 arcminutes. The detector area outside the central 70 mm part is used as a "veto–ring" for rejecting background events. LEPC covers the 0.2–8 keV range, but the positioning of the energy range can be changed upwards in energy. An alternative operating mode with a LEPC energy range of 0.5–16 keV can thus be chosen. The LEPC quantum efficiency including the window transmission is shown in Fig. (4.3). The window support grid results in about 25% absorption independent of energy. Below 1 keV the LEPC quantum efficiency is reduced by absorption in the window. However, the thin window of LEPC (0.85 μm) ensures an observation window between 0.2 and 0.28 keV (the C edge) which is well suited for the ML crystals on the Objective Crystal Spectrometer.

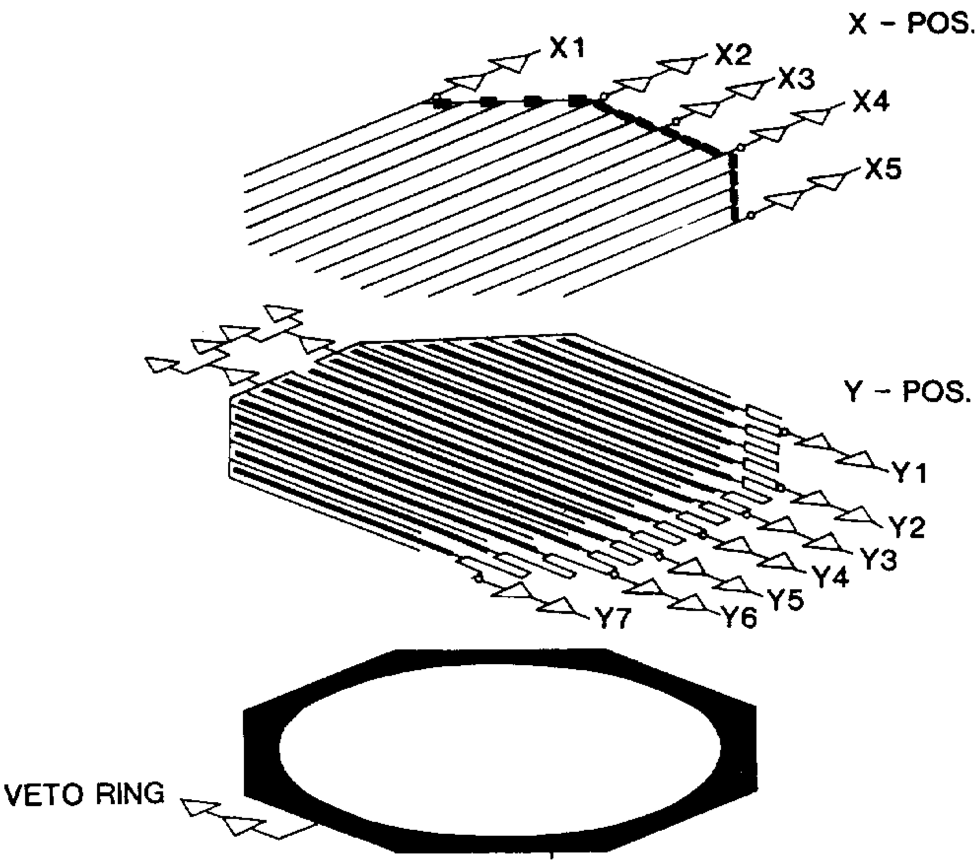

Figure 4.1: Wire grid and micro strips with read–out nodes and "veto ring" of one HEPC. See the text for details.

HEPC specific matters

The HEPC micro strip plate is octogonal and has a diameter of 160 mm. The entrance window is circular with a diameter of 150 mm giving a circular FOV with a diameter of 60 arcminutes. The detector area outside the central 150 mm is used as a "veto–ring" for rejecting background events. HEPC covers the 2–25 keV range, see Fig. (4.4). At the high energies the quantum efficiency drops because the gas becomes transparent to X-ray photons and the decrease at the low energies is due to the window absorption.

XRT plus LEPC/HEPC spectral response

In Fig. (4.5) the effective area of one XRT together with one XRT plus one LEPC/HEPC is shown. The gold coating of the XRT produces the absorption edge just above 2 keV. Together the LEPC and the HEPC covers the energy range 0.2–20 keV with an effective area above several times 100 cm^2 in most of this range.

The spectral resolution of the LEPC and the HEPC is found to vary as the square

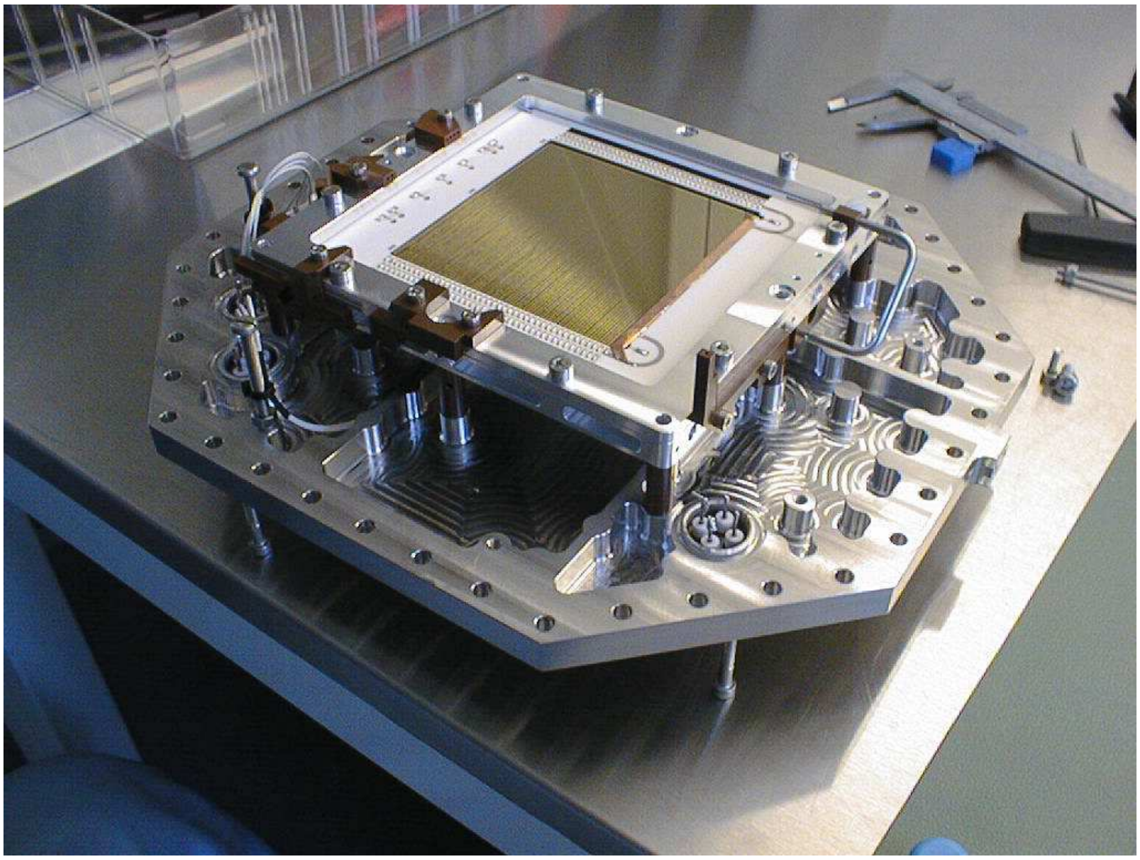

Figure 4.2: LEPC micro strip plate mounted in detector box.

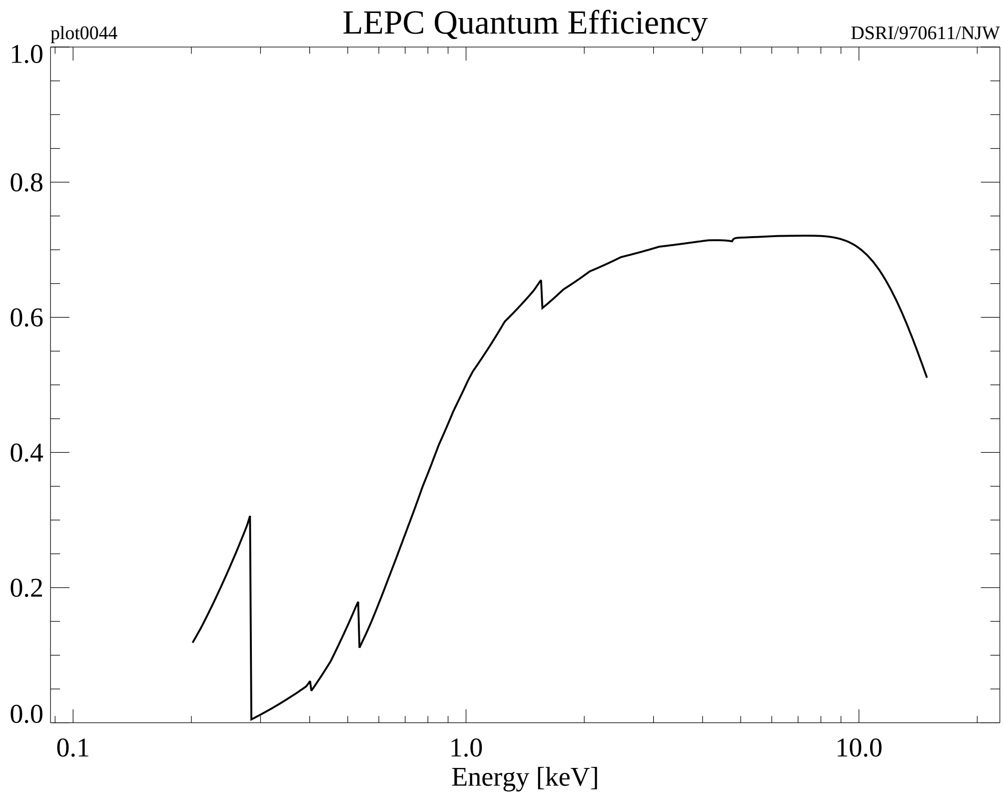

Figure 4.3: LEPC quantum efficiency including window transmission. Note that only the 0.2–8 keV range or the 0.5–16 keV range can be chosen – the full range is shown.

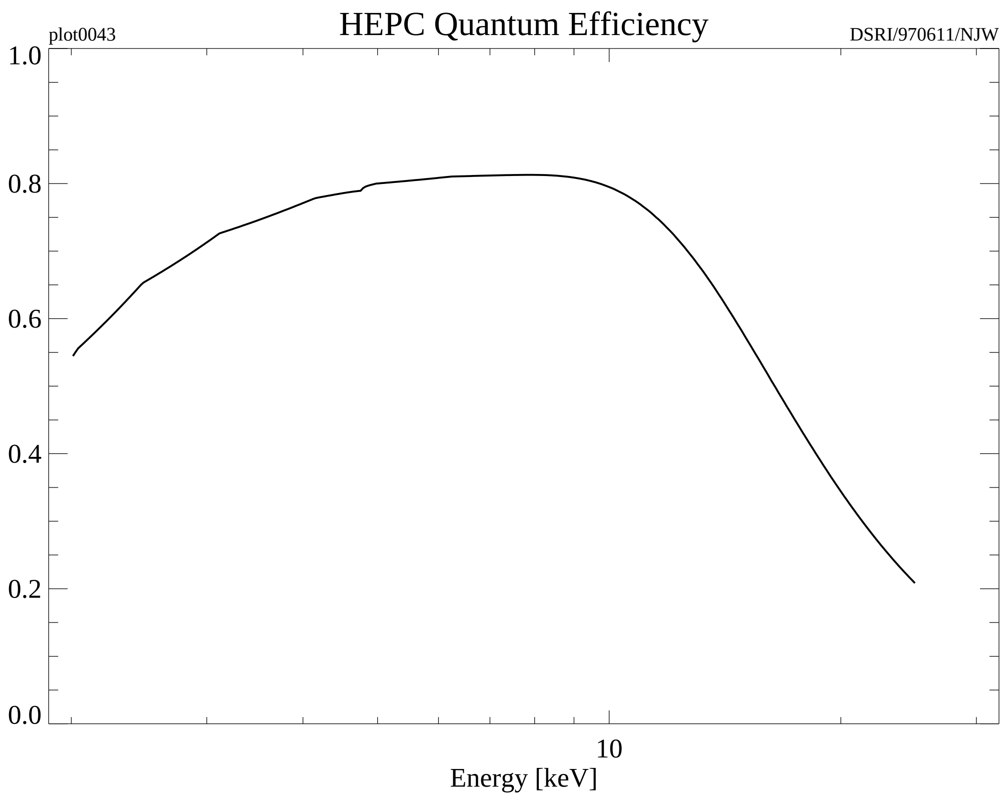

Figure 4.4: HEPC quantum efficiency including window transmission.

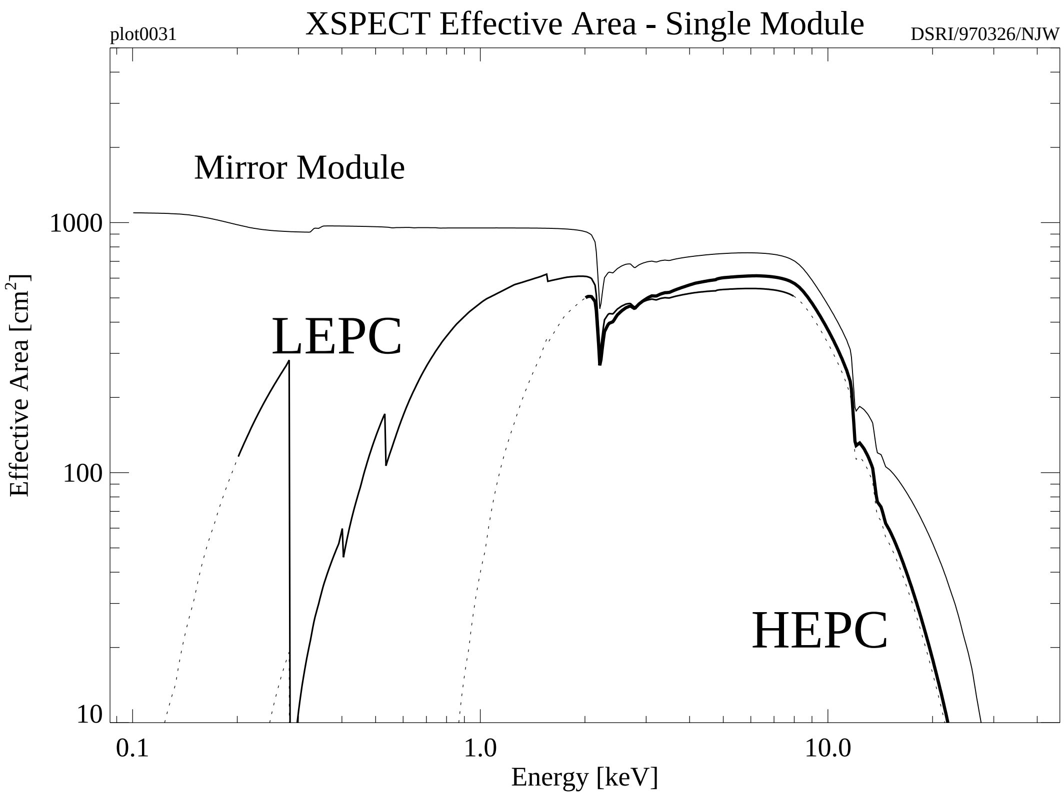

Figure 4.5: On–axis effective area of one XRT plus LEPC/HEPC.

root of the energy:

$$\Delta E(FWHM) = 0.33 \times \sqrt{\frac{E}{1keV}}\ keV \tag{4.1}$$

At 1 keV the relative energy resolution is 33%, decreasing to to 13% at 6 keV and to 10% at 10 keV.

Position determination

The micro strips can be placed much closer than the wires in conventional proportional counters, almost eliminating spatial non–linearities in the position response of LEPC/-HEPC. Positions are determined by the principle of charge division. Resistors are deposited on the micro strip plate in a "zig–zag"ish pattern of Au which is connected to each cathode strip. The resistive chain is subdivided into six sections by six read–out nodes. Each wire of the grid is connected to the adjacent wires through laser trimmed thick–film resistors on the ceramic frame. The grid resistor chain is subdivided into four sections by four read–out nodes. Due to diffusion in the counter gas, the primary electron cloud from an X–ray event will have a diameter of a few mm on the micro strip plate and will therefore produce signals in two or three read–out nodes. From the charge distribution on read–out nodes the position of the X–ray event can be calculated. The position accuracy is better than 2 mm in the LEPC/HEPC energy range and better than 1 mm in most of the range, see Fig. (4.6).

In the XRT focal plane 1 mm corresponds to 0.5 arcminute so the detector position accuracy is negligible compared to the XRT PSF with a HPC of ~ 3 arcminutes.

Timing

The intrinsic time resolution of LEPC/HEPC is 1 μs. In orbit the timing is made relative to the satellite clock and at present it is not quite clear how accurately this can be done. However, the time stamps associated with each event is at best expected to be accurate to 2–3 μs relative to the satellite clock, dependent on the chosen time format. Post–facto the absolute time (UT) will be derived and this is expected to be accurate to about 1 ms.

Background

Detector background arises first of all from charged particles crossing the detector. They produce an extended ionization track which results in a pulse with a rise time given essentially by the time it takes the primary electrons to drift to the amplification stage. X–rays, in contrast, produce a localised charge cloud with a much shorter pulse rise time. Based on a measure of their rise time and an anti–coincidence technique, background events are rejected. From laboratory measurements of the cosmic ray background it is estimated that a rejection efficiency of $> 99.9\%$ can be achieved for both the LEPC and the HEPC. For the SRG orbit the direct particle background is then reduced to $< 1{\times}10^{-4}$ cm^{-2} s^{-1} keV^{-1}.

Other sources of detector background include high energy photons from the cosmic X–ray background and neutrons produced by cosmic ray interactions with the satellite structure. These particle induced events are indistinguishable from X–ray events in the

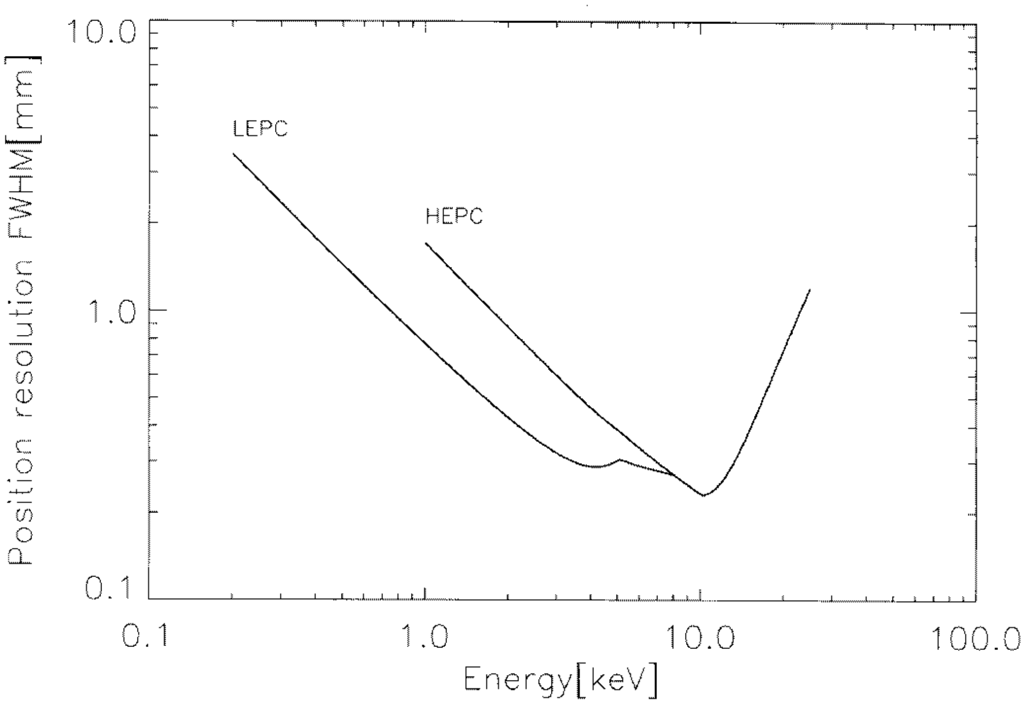

Figure 4.6: Position resolution for LEPC/HEPC. In the XSPECT focal plane 1 mm corresponds to $0.5'$.

LEPC/HEPC range and prelimenary calculations predict a rate of $\sim 5{\times}10^{-4}$ cm^{-2} s^{-1} keV^{-1}. Due to the unknown details of the cosmic ray interaction with the SRG satellite this rate is uncertain with about a factor two.

Finally, it must be kept in mind that the X–ray sky background adds to the detector background.

Detector operations and data formats

The operations of LEPC/HEPC is controlled through a number of parameters specifying which events to accept and which information to record for each event. For most observations, the default settings of these parameters will be adequate, but for specific purposes the detectors may be operated with different settings.

LEPC/HEPC can handle up to 3000 cts/s – for brighter sources correction for dead–time in the detectors becomes large. Furthermore, the on–board memory will be filled up if a bright source is observed for a long time and all event information is recorded. For each detector, 80 Mbyte can be stored on disks on–board between two ground contacts.

This constraint imposes restrictions on the information which can be recorded for each event. The following criteria for accepting/rejecting events can be applied:

- **Position mask:**
  A rectangular position mask on the detector can be specified by the positions of the four corners. Events within the rectangle may be accepted or rejected.
  This option is particularly useful in case of a very bright source close to the target. The bright source may fill up the on–board memory during the observation so it will have to be masked out before target data can be taken.

- **Background rejection:**
  The criteria for rejecting background events on–board may be changed. For instance, for studies of very faint sources (such as the cosmic X–ray background) this option could be relevant.

- **Energy window:**
  The energy window within which events are accepted can be narrowed in. This may be applied (especially for a bright source) if a specific feature in the spectrum is to be studied.

- **Dynamic range of LEPC:**
  The LEPC energy range can be shifted from the nominal 0.2–8 keV to 0.5–16 keV.

For the detailed setting of the above mentioned parameters, please contact M.Møhl Madsen (mmm@dsri.dk).

Events detected by LEPC/HEPC can be recorded in 7 pre–defined data formats, (see Appendix for the details of these formats): Raw, A1, A2, B1, B2, D1 and I format. Only one of these formats can be chosen for a given observation. Selecting the optimum data format depends on the expected count rate and the scientific questions to be addressed. Of the 80 Mb on–board memory, some must be reserved for "house keeping" data of the detector and the satellite, leaving about 78 Mb for scientific data between two ground contacts. Events from the background take up part of this, leaving some fraction of 78 Mb for target events, depending on the chosen data format. See the chapter, "Feasibility considerations and observation planning" for details on how to choose the most suitable data format.

Calibrations of LEPC/HEPC

During the PV phase of SRG, a number of calibration measurements will be carried out for verifying the performance of the LEPC and the HEPC. At the back of this Handbook, a list of the measurements planned for the PV phase is given.

Each LEPC/HEPC contains its own internal ^{55}Fe calibration source emitting 5.9 keV X–rays onto the detector outside the FOV. Thus the gas gain can be monitored and some information on the LEPC/HEPC energy response can be obtained. Furthermore, when not in the foca of the XRTs, the full active area of LEPC and HEPC can be illuminated with X–rays from a number of ^{55}Fe sources through a multiple collimator. This produces 62 point like spots within the central 150 mm of HEPC and 33 point like spots within the central 70 mm of LEPC. From these, the LEPC and the HEPC position response, energy response, detector efficiency and background rejection efficiency can be determined. Before and after an observation, an exposure under the calibration sources can be requested for testing the detector performance.

Summary of LEPC/HEPC characteristics

The characteristics of the LEPC and HEPC detectors are summarised in Table (4.1).

Detector	HEPC	LEPC
Gas	Xe + 10% CH4	Xe + 10% CH4
Pressure	1.0 bar	1.0 bar
Window material	Polyimide	Polyimide
Window thickness	7.5 μm	0.85 μm
Support grid	W mesh	W mesh
Field of view	Circular Ø=60′	Circular Ø=30′
Energy range	2–25 keV	0.2–8 keV (0.5–16 keV)
Energy resol. @ 6 keV	13% FWHM	14 % FWHM
Max. count rate	3000 counts/s	3000 counts/s
Available on–board memory	80 Mbytes/24 h	80 Mbytes/24 h

Table 4.1: Characteristics of the LEPC/HEPC detectors.

The Objective Crystal Spectrometer

Design principles and method of operations

In front of one of the mirror systems a Bragg panel, the Objective Crystal Spectrometer (OCS), is placed. The OCS can be regarded as a narrow filter only transmitting photons with an energy selected by the Bragg relation for the given positioning of OCS panel relative to source and detector. Each position in the focal plane satisfies a specific Bragg angle on the crystal and therefore, each pixel on the detector corresponds to a particular energy and direction, see Fig. (5.1). By turning the OCS panel an energy range is scanned with a spectral resolution defined by the quality of the crystals, i.e. in the eV range. For scanning a spectral range with a reasonable sensitivity the telescope optical axis must also be re–oriented. This is due to shadowing from the entrance to the OCS panel and the vignetting of the telescope (see below). In this way, for a point source a very high resolution spectrum is obtained while for an extended source, energy resolved images are obtained.
For extensive descriptions of the OCS we refer to Schnopper and Byrnak (1987); Schnopper (1994); Christensen et al. (1994); Wiebicke et al. (1997).

The OCS consists of a flat nearly circular panel of dimensions 650 mm$\times$610 mm, i.e. almost the same size as the diameter of mirror system. The panel is made of two “skin” plates of aluminum and the crystal mosaics are glued on the “outer” side. On the “inner” sides heaters and thermal sensors are placed and in between the “skin” plates a rotation axle (perpendicular to the telescope viewing direction) is fixed to the panel. The whole unit is installed in a carbon fiber epoxy tube mounted on top of the SODART telescopes. A door in the side of the tube can be opened and allow photons from a source about 90° from the general viewing direction to be reflected off the panel and down through the telescope, see Fig. (5.2). When the OCS panel is not used, it is turned so it is parallel to the telescope optical axis.

OCS crystals

Three different crystal arrays are glued to the panel. One side is completely covered with LiF(220) crystals, the other side is partly covered with Si(111) crystals and partly with RAP(001) crystals. Half of the mosaic on both the Si–/RAP–crystal side of the panel is shown in Fig. (5.3).

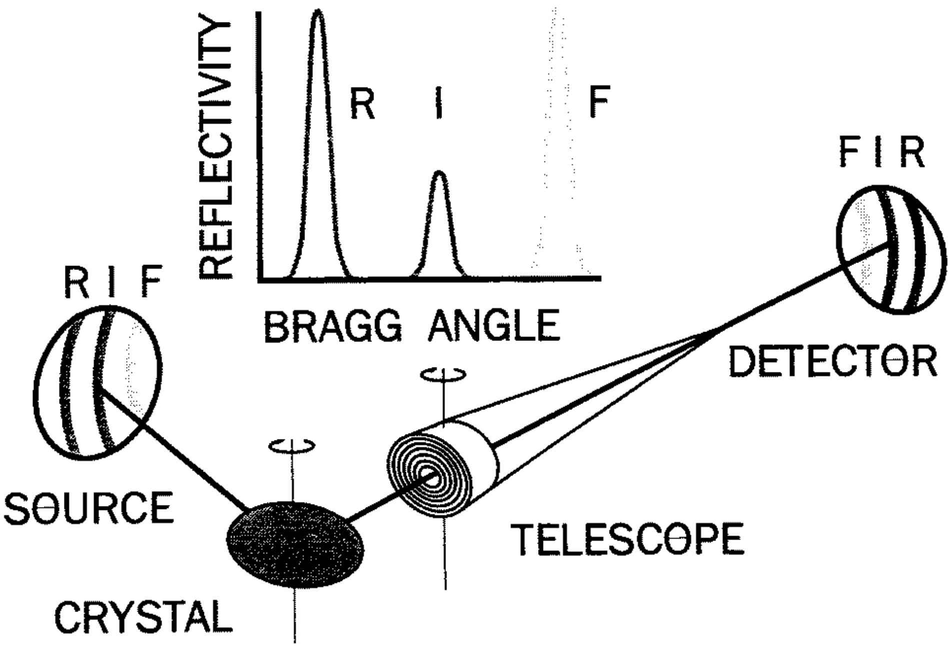

Figure 5.1: The OCS concept. From Schnopper (1994).

Furthermore, the Si crystals have been coated with Co/C multilayers, allowing spectroscopy below the C–edge at 0.285 keV. Softer X–rays are reflected in the multilayer coating and harder X–rays are reflected in the Si crystal.

Each type of crystal allows high resolution spectroscopy in a given energy range (see Fig. (5.4)): LiF (5–10 keV), Si (2.5–5 keV), RAP (0.6–1.2) keV. The multilayers are sensitive in the (0.2–0.285 keV) range. Note that these are not "hard" limits, but depend on the desired sensitivity. These energy ranges have been chosen so as to cover H– and He–like line emission from Fe, Si, Ne, Ca, S, Ar and O, and line emission below the carbon absorption edge at 0.285 keV. For studies below 0.285 keV it must be kept in mind, that such low energy photons are subject to heavy absorption in the galactic interstellar medium and that this is strongly dependent on the given line–of–sight.

The side of the OCS panel with Si– and RAP–crystals and multilayers enables simultaneous studies of lines in different energy ranges. For the same Bragg angle, reflections from both of the crystals and from the multilayers can be separated based on the energy of reflected photons. The spectral resolution of the LEPC detectors is sufficient for this purpose. In this way the efficiency of the OCS can be doubled or even tripled for sources where several lines within the OCS ranges are to be studied.

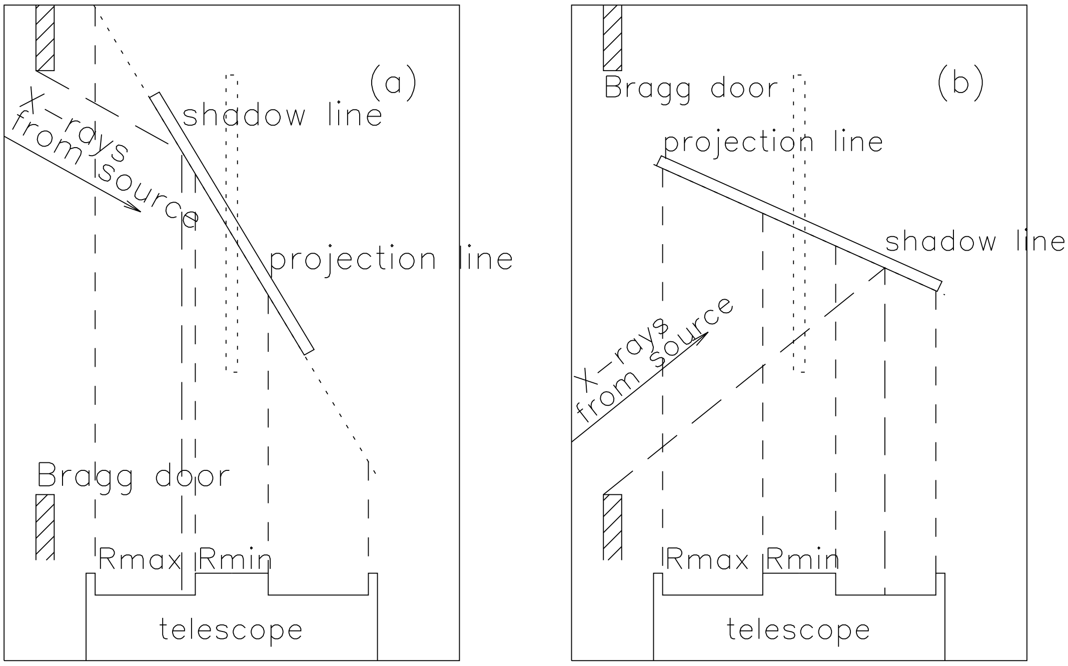

Figure 5.2: Position of the OCS panel relavite to the entrance door and the XRT. β is the Bragg angle and $R_{\rm min}$, $R_{\rm min}$ is the inner and outer radius of the XRT respectively. The OCS panel in the position when it is not in use is outlined in dotted typestyle. Long dashed lines mark shadowing lines from the entrance door and short dashed lines mark shadowing lines from the XRT. a) Bragg angle = 30° and b) Bragg angle = 65°. From Wiebicke et al. (1997).

The OCS response function

The ingredients for calculating the OCS response for a specific source–OCS panel–telescope geometry to a source with a given spectrum and a given surface brightness distribution are:

- A geometrical factor accounting for:
  - Shadowing by the OCS panel entrance door – for Bragg angles smaller than 41° or larger than 60°, see Fig. (5.2).
  - Not all incident photons hit a crystal of the desired type.
  - Not all Bragg reflected photons fall into the XRT FOV.
- Reflection off Bragg crystals (rocking curve).
- Telescope effective area as function of position in FOV and energy of incoming photon.
- Detector efficiency.

The details of the OCS response calculation can be found in Wiebicke et al. (1997). A program for calculating the OCS response function has been developed by Ingolf Halm and the results for each of the four OCS energy bands are shown in Fig. (5.4).

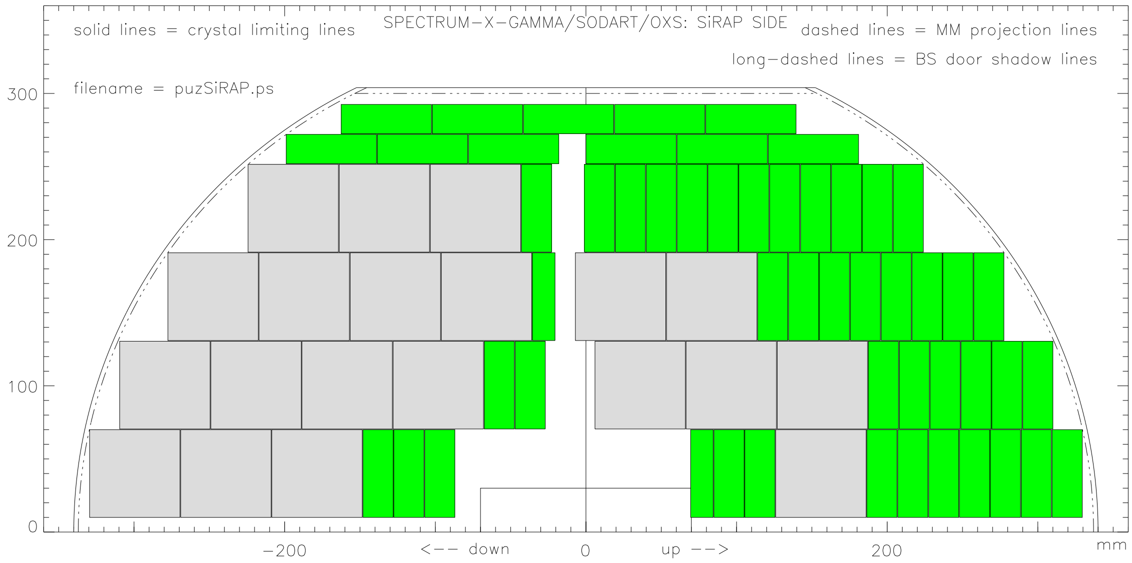

Figure 5.3: Half of the side of the OCS panel covered with a mosaic of Si– (light and square) and RAP–crystals (dark and rectangular). Courtesy Hans Wiebicke and Ingolf Halm, AIP.

The units of the OCS response given here are such that the count rate for a given source is obtained by multiplying the response at the relevant energy by the source flux in units of photons/s/cm^2/keV. These responses have been conformed to the XSPEC spectral fitting programme format for running simulations of OCS observations. The OCS response calculation programme can be obtained by contacting Ingolf Halm (ihalm@aip.de). Furthermore the OCS response will be included in the UM_TOOL simulation package which is publically available at the DSRI home–page. See the chapter "Simulating observations" for more details on how to use UM_TOOL.

OCS energy resolution

The energy resolution of the OCS is determined by the quality of the Bragg crystals (the rocking curve) and the accuracy with which the crystals are glued to the panel. In Fig. (5.5) the energy resolution calculated from the rocking curve is shown as function of energy for the four OCS energy ranges.

Multilayers and LiF crystals have a resolution around 1–10 eV while RAP crystals give energy resolutions around 1 eV and Si crystals about 0.5 eV.

Once the flight OCS panel has been completed the accuracy of the glueing will be measured. Prelimenary results show that the rocking curve is the major contributor to the energy resolution.

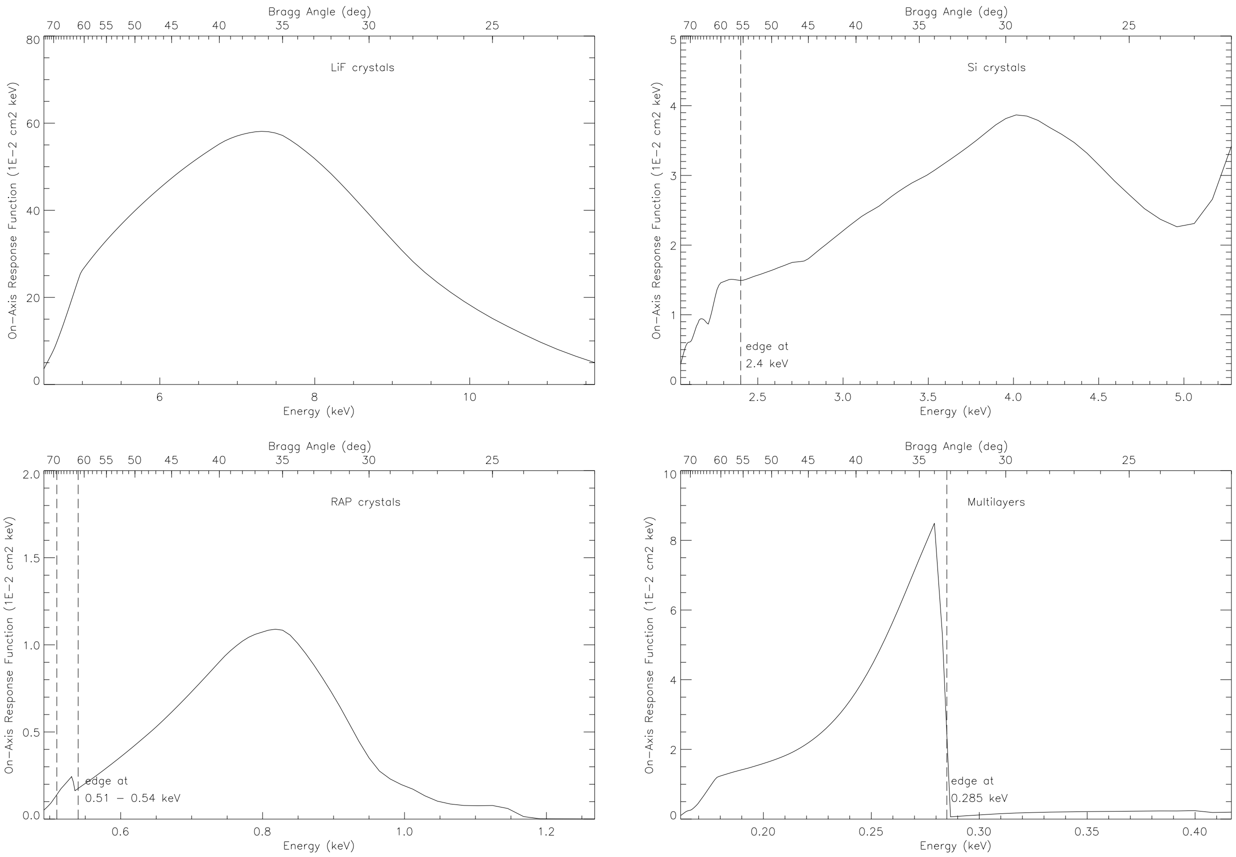

Figure 5.4: Response of the OCS in the four available energy ranges. On top is given the Bragg angle corresponding to the energy at the first axis. The dashed vertical lines indicate absorption edges, hampering spectroscopy at these particular energies. Courtesy Hans Wiebicke and Ingolf Halm, AIP.

Operating the OCS

For a full observation, the response for each source–OCS panel–telescope geometry must be added to form an estimated spectrum or energy resolved images. In order to scan an energy range for a given source on the sky, the OCS panel has to be turned and the telescope optical axis must be re–oriented several times. Hence, the detailed manoeuvering of the OCS panel and the satellite during a typical observation is quite complicated. A typical OCS observation consists of a number of telescope orientations and for each of these, a range of Bragg angles are scanned. For each telescope pointing, the following parameters must be specified (the numbers in brackets are the accuracy with which the parameters can be determined and hence the accuracy to which they must be specified):

- Pointing direction ($0.5'$).
- Start Bragg angle ($0.5'$).
- Step size of Bragg angle ($0.5'$).
- Number of steps (1 to 1000).

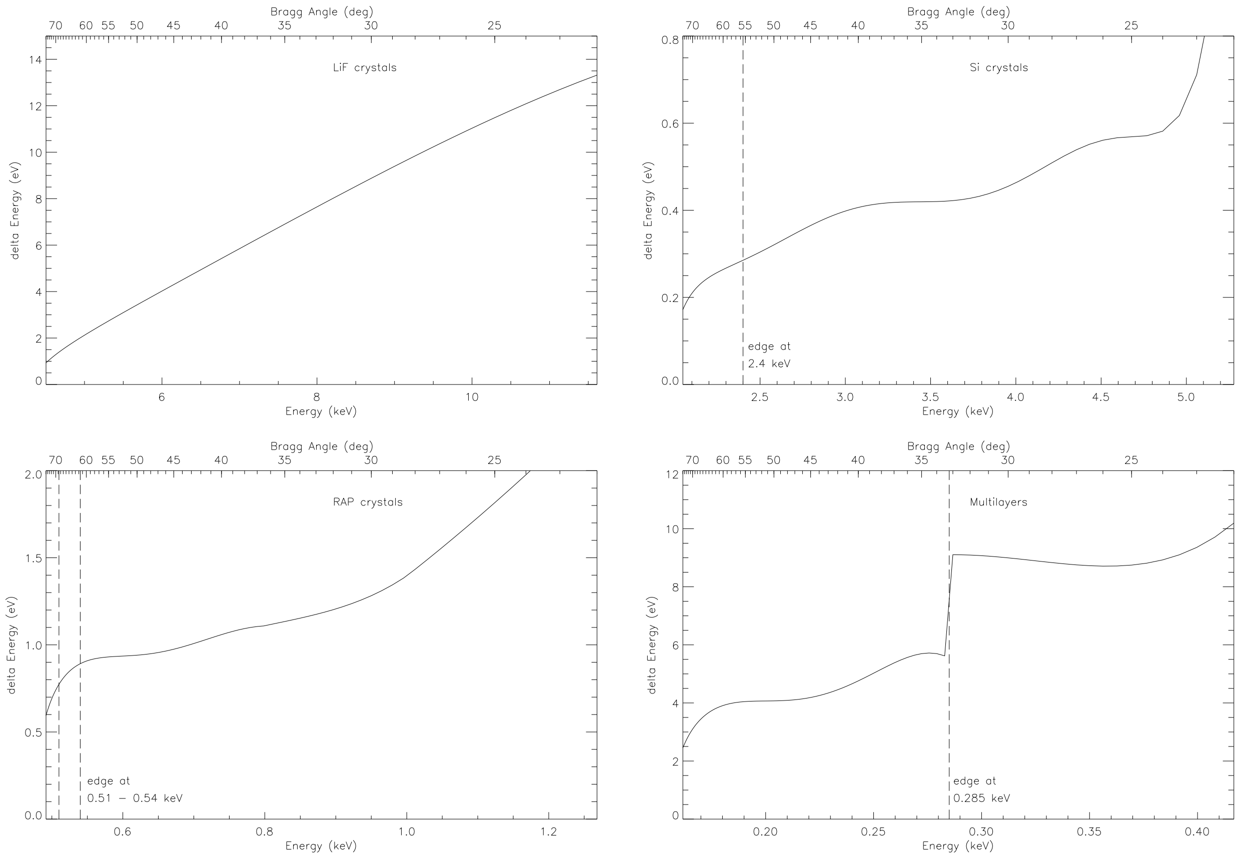

Figure 5.5: Energy resolution as function of energy for the four OCS energy bands. On top is given the Bragg angle corresponding to the energy at the first axis. The dashed vertical lines indicate absorption edges, hampering spectroscopy at these particular energies. Courtesy Hans Wiebicke and Ingolf Halm, AIP.

- Exposure time for each step (100 s to 10000 s).

Up to 10 re–orientations of the satellite per 24 hours can be done. However, even the brightest sources require long exposure times per pointing direction so this is not a severe constraint.

Feasibility considerations and observation planning

In this chapter we go through the considerations one has to make in order to estimate the feasibility of XSPECT observations of a given source. In the chapter "Simulating observations" the details on how to estimate the results of an observation can be found.

The constraints imposed by the orbit and the satellite operations are presented in the chapter "Spectrum–Røntgen–Gamma overview".

In the chapter "The LEPC and HEPC detectors" details about the detector operations are given.

OCS operations are discussed in the chapter "The Objective Crystal Spectrometer".

Targets of opportunity observations

The policy for how to decide for target of opportunity observations (TOOs) have not been finally agreed upon. However, a maximum allocation of time to TOOs in any one year has been fixed to be 5%. The time from a TOO is requested to SRG can be pointing at the desired target will be a few days.

Pointing direction and roll angle

For any observation, the pointing direction must be specified in equatorial coordinates (α, δ). The pointing direction (accurate to $35''$) and the pointing stability of the satellite is better than the HPD of the telescopes. Data from TAUVEX could be used to re–construct the pointing direction post–facto, possibly to $5''$ accuracy. As a consequence, the pointing direction should be specified to at least $35''$ and preferentially to $5''$.

In order to better separate the vignetting effects of the telescope from a surface brightness fall–off of the target, it is beneficial to off–set the target a few arcminutes from the optical axis. This is especially the case for extended sources. Furthermore, special care in choosing the pointing direction must be taken for target(s) showing extended structure or if XSPECT observations would benefit from being combined with data from JET-X, having a smaller FOV.

Once the pointing direction is specified, the turning of the XRT around the optical axis (roll angle) must be determined. The roll angle can not be chosen freely due to the restrictions on the satellite pointing direction. However, for any given observing time and pointing direction, there is an allowed range of roll angles. If XSPECT data are to be combined with JET-X data, it is important to choose the optimum roll angle for having the target(s) within the rectangular JET-X FOV. Due to the observing time dependence on the possible roll angles, for a given observation, the roll angle can not be speficied by the observer until the observation schedule is fixed. The program JMAN can be used to estimate the available observing window for a given position, see the list on "Other sources of information" at the back of this Handbook.

Detector combination

First of all, the combination of detectors for the two telescopes must be decided. Any of the combinations LEPC+HEPC, LEPC+SIXA, HEPC+SIXA, LEPC+LEPC, HEPC+HEPC can be chosen. Furthermore, for one pointing it is possible to combine SIXA with LEPC for some part of the observing time and with HEPC for the remaining part of the observing time. The sledge in the focal plane is moved during the pointing for exchanging LEPC/HEPC. If this option is chosen, the individual LEPC and HEPC observing times must be specified.

For imaging purposes, LEPC/HEPC is superior to SIXA so if imaging is the main issue, a combination of LEPC/HEPC would be the preferred choice. The spectral resolution of SIXA is superior to LEPC/HEPC so for spectroscopy or a combination of spectroscopy and imaging a combination of SIXA and HEPC/LEPC would be preferred (unless the spectral feature to be studied is outside the SIXA energy range).

The target(s) in question should of course be within the detector FOV. Both LEPC and HEPC have circular FOVs, but the diameter of the LEPC FOV is $30'$ while the HEPC FOV is $60'$. The SIXA FOV consists of 19 circular pixels with a diameter of $3.9'$ and gaps in between the pixels, making SIXA less well suited for imaging. So for objects extending more than about $20'$, HEPC is the preferred detector unless the low energy sensitivity is important. Both LEPC and HEPC images are 256 pixels by 256 pixels.

Imaging

A number of matters related both to the XRT and the detectors must be discussed when considering/planning imaging with XSPECT. The driving force is of course the nature of the target(s) to be studied: How large is the target(s)? Can the target(s) be resolved? If so, what is the expected surface brightness distribution? What is the expected count rate of the target(s) relative to the expected background count rate? Are there any confusing sources close to the target(s)? In order to deal with these questions, at least the following issues must be addressed.

- **Point spread function.** The HPD of the XRT PSF is much larger than the accuracy of the position determination in LEPC/HEPC making the effects of the detector position determination negligible. The PSF has a sharp core with wide wings. This means that photons originating from different directions on the sky are mixed in the focal plane. Furthermore, the XRT PSF depends on energy as well as position in the FOV. These effects taken together make direct deconvolution of images very difficult. Also, spatially resolved spectroscopy must take the mixing of photons into account. For deep exposures ($\sim 10^5$ s), there will be several sources at about the detection limit within the PSF HPD. This causes "confusion" and the flux from what seems to be just one source is the sum of fluxes from several sources. When "confusion" sets in is dependent on energy; "confusion" is more of a problem at the low energies. The "confusion" limit at 9 keV calculated as in Condon (1974) is (dependent on the assumed distribution function of sources) a few times 10^{-14} erg/cm^2/s. This problem can be alleviated by combining XSPECT data with the better spatial resolution of JET-X data.

- **Vignetting.** Vignetting is the decrease of sensitivity with distance from the XRT optical axis. Hence the ability to detect a source decreases with its off-axis distance. Furthermore, the vignetting is energy dependent which especially must be taken into account when analysing images of extended sources.

- **"Stray light".** X–ray photons originating outside the FOV can scatter off the back sides of the XRT foils and into the FOV ("stray light"). This effect is strongly dependent on the energy of the incident photon, being important only at energies < 2 keV. When studying a faint source in the FOV with a bright source located just outside the XRT FOV, a large fraction of the detected counts can originate from the bright source. This can inhibit proper analysis of the faint source so this situation should be avoided as much as possible. For studies of the cosmic X–ray background (CXRB), there will always be a non–negligible contribution from the CXRB outside the FOV to the CXRB counts within the FOV. Also, the CXRB spectrum will be distorted because of the "stray light" energy dependence.

- **Masking.** When studying a faint source near a bright source, it can be useful to mask out the bright source or to accept counts from a region around the faint source only. In this way it can be prevented that the bright source fills up all the available on–board memory. For this option, the corner positions of a rectangular mask must be specified. However, even with masking some photons from the bright source will still fall on the same spot of the detector as photons from the faint source due to the width of the PSF.

- **Background rejection.** The criteria for rejecting background X–ray photons can be changed upon request. For special cases, this could improve the image quality.

- **Raster scans.** For covering an area significantly larger than the HEPC FOV raster scans can be made. This option is particularly useful for bright, extended sources or surveys.

Spectroscopy

The driving force for deciding how the spectroscopy should be carried out is of course the nature of the target(s) to be studied: Which spectral features are interesting for the target(s) in question? Continuum, particular lines, particular absorption edges? Which spectral resolution is needed in order to address the scientific issues in question? What is the expected count rate relative to the expected background count rate? Are there any confusing sources close to the target(s)? The instrument properties to bear in mind are:

- **Spectra of close sources.** Due to the wide wings of the PSF, photons from two nearby sources on the sky will be mixed in the focal plane. Hence the spectrum from one of the sources is "polluted" with emission from the other source and the degree of "pollution" is a function of energy. In this way spectral analysis and spatial analysis are mutually linked.

- **Absorption edges in instruments**. Spectroscopy near the absorption edges from the XRT+detector is difficult since it is very hard to calibrate the exact XRT+detector response at the edges. The most prominent edges are Au(2.2 keV) and C(0.285 keV).

- **Masking.** As discussed in the "Imaging" section, studiying a faint source nearby a bright source is possible by masking out the bright source. However, the spectrum of the faint source will still be "polluted" by photons from the bright source.

- **Background rejection.** The "standard" background rejection criteria may be changed upon request. For instance, one could hope to optimize the rejection criteria for improving spectra of the CXRB.

- **Narrowing energy range.** For LEPC and HEPC a narrower energy range than the full range can be chosen. If a special spectral feature is to be studied for a bright source, this could be a useful option.

- **Changing LEPC energy range.** The LEPC energy range can be changed upwards to 0.5–16 keV. For some sources, emission below 0.5 keV may be less interesting than going to energies above 8 keV with the same detector.

Timing

The intrinsic time resolution of LEPC/HEPC is 1 μs. In orbit the timing is made relative to the satellite clock and current best estimates suggest an accuracy of 2–3 μs. However, the accuracy of the time stamps of each event depends on the chosen data format. The RAW format gives the most accurate time, that is in units of 1 μs. In Table (6.1) the timing accuracy relative to the satellite clock for the different data formats are given. The absolute time (UT) derived post–facto is expected to be accurate to about 1 ms.

Estimating exposure time

The exposure time for a given target must be decided on basis of the science to be extracted from the data, subject to the limitations of the satellite and the detectors. In almost any case "the longer exposure time, the better" so the key question is: What is a *sufficient* exposure time for extracting the desired information from the data?

Background

First of all, the level of the background must be estimated for the given source. The background consists of the detector background (particle background) and the cosmic X–ray background (CXRB). Below 1 keV the galactic X–ray emission dominates the CXRB and this component varies on a degree scale with up to a factor of five. The galactic X–ray emission is well fitted with thermal bremsstrahlung model with temperature kT$\sim$ 0.15 keV. Above 1 keV the extra–galactic X–ray background dominates and ASCA studies have shown that this is well represented as a power law with index Γ = 1.4 in the range 1–7 keV. In Fig. (6.1) the estimated total background count rate as function of energy is shown for HEPC.

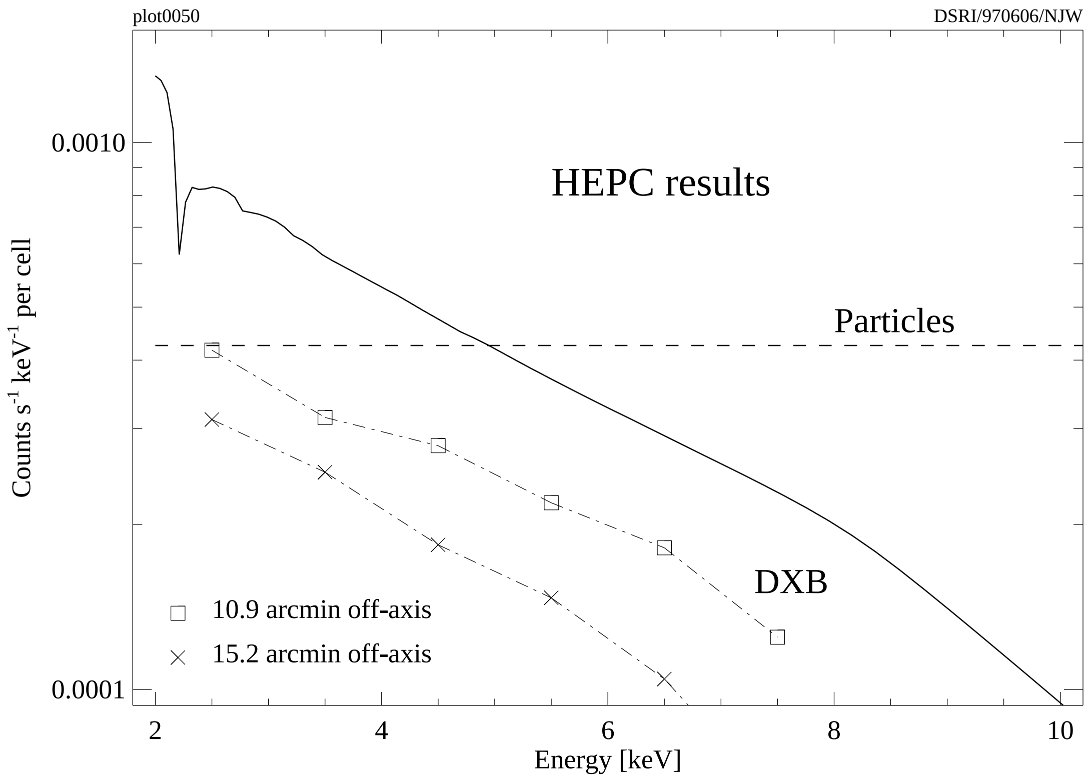

Figure 6.1: The background rate in HEPC as a function of energy for a circular area on the detector with the XRT HPD=3 arcminutes as diameter. The estimated particle count rate (direct plus induced) is shown as a dashed line. It will be almost independent of energy and position in the detector. The cosmic X-ray Background (DXB) will, however, depend on the off-axis angle and two examples are shown. The curves have been derived by a Monte-Carlo raytracing method which includes some statistical noise in the values.

On-axis, the particle background dominates above 5 keV while off–axis it is dominant for all HEPC relevant energies. For HEPC, the total background count rate within the FOV is estimated to be 5 counts/s and for LEPC it is about 2 counts/s.

Detection limits

The question is typically: Given an expected source flux and an estimate of the background flux, how long exposure time is needed for a 5σ detection? In Fig. (6.2) is given the minimum detectable flux by HEPC in an energy interval with a width equal to the detector resolution as function of exposure time. Scaled down Crab spectra ($9.7 \times E^{-2.1}$ photons/s/cm^2/keV) are shown for reference.

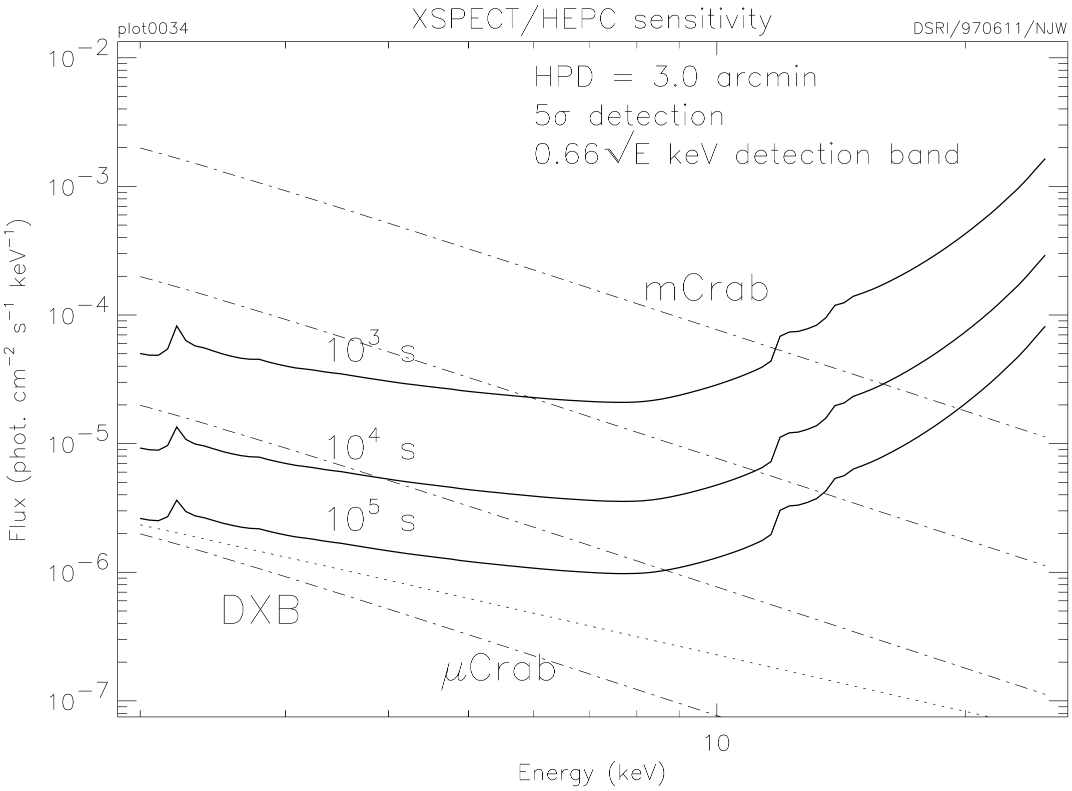

Figure 6.2: The thick curves show the on-axis minimum detectable (5 σ) flux as a function of energy with HEPC in the focus. The exposure times are marked on the three curves. The photons in the Half-Power-Diameter (HPD) are used and an energy band which is twice the FWHM of the detector resolution. For comparison spectra similar to the Crab spectrum but at the intensity indicated have been shown as well as the Diffuse X-ray Background (DXB, dotted line) inside the HPD. Courtesy Niels Jørgen Westergaard.

In an exposure time of 10^4 s a 0.1 mCrab spectrum out to 10 keV can be obtained. To go down to 0.01 mCrab out to 10 keV an exposure time of 10^5 s is required.

In Fig. (6.3) is shown the corresponding plot for LEPC.

In the LEPC energy range, a 10^4 s exposure is enough for a 5 σ detection of a 0.1 mCrab spectrum.

Note that the above plots give the on–axis sensitivity. When going off–axis, the vignetting of the XRT must be taken into account, decreasing the sensitivity.

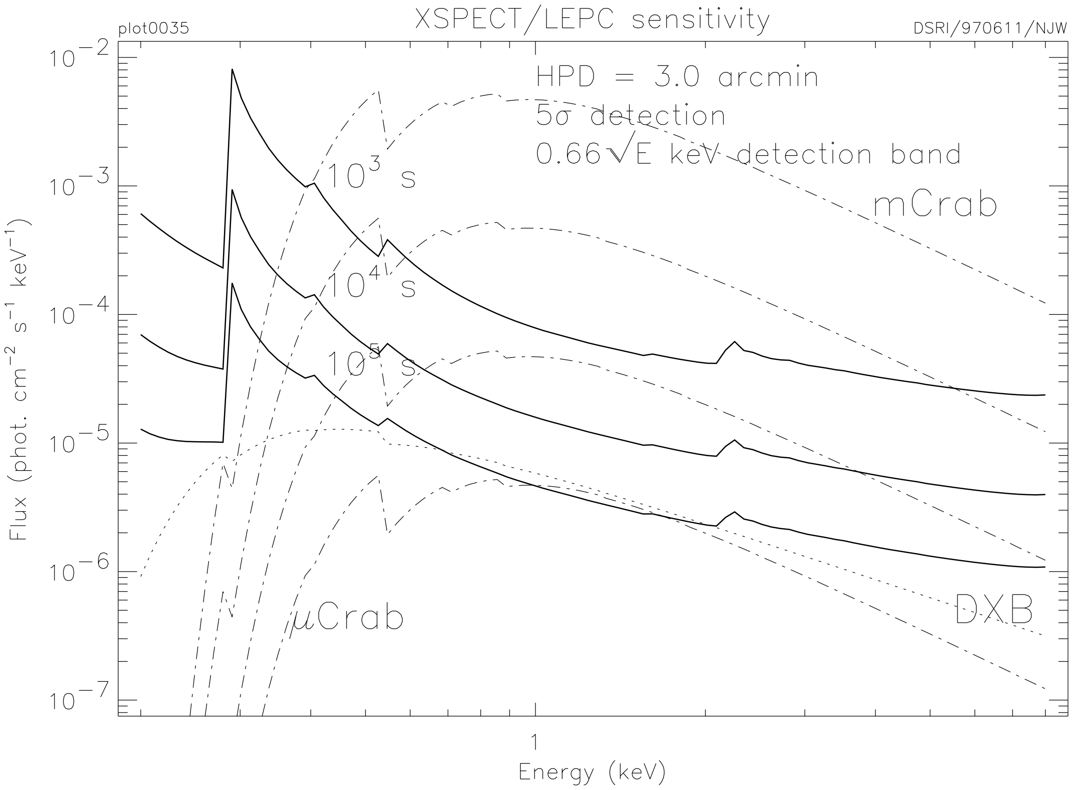

Figure 6.3: The thick curves show the on-axis minimum detectable (5 σ) flux as a function of energy with LEPC in the focus. The exposure times are marked on the three curves. The photons in the Half-Power-Diameter (HPD) are used and an energy band which is twice the FWHM of the detector resolution. For comparison spectra similar to the Crab spectrum but at the intensity indicated have been shown as well as the Diffuse X-ray Background inside the HPD. Courtesy Niels Jørgen Westergaard.

In order to simulate the detailed appearance of a spectrum, UM_TOOL or XSPEC can be used (see the chapter "Simulating observations"). UM_TOOL also provides the expected count rate for a given exposure time or conversely the estimated exposure time for a detection.

Satellite constraints

The scientific judgement of a "sufficient" exposure time must also comply with the operational constraints of the satellite. Exposure times for individual pointings can not be longer than the time between two ground contacts, i.e. about 10^5 s. There is no lower limit on the exposure time, but since the number or re–orientations of the satellite between two ground contacts is limited to about 10, only a small number of very short exposures can be accomodated between any two ground contacts. It is however possible to make raster scans within a single observation by scanning an area on the sky by many short exposure pointings.

Choosing LEPC/HEPC data format

With a given spectral model for the target, the simulation tools UM_TOOL and XSPEC can be used to estimate the count rate for a given detector. For count rates above 3000 counts/s, LEPC/HEPC dead–time corrections become very large, hampering data analysis. Furthermore the 78 Mb data storage capacity per detector constrains which data formats that can be used for a source with a given count rate. Background events inevitably take up some fraction of this memory and how much depends on the pointing direction and the data format. On average about 2 counts/s is expected for the full LEPC energy range and about 5 counts/s is expected for the full HEPC energy range. However, it must be kept in mind that these numbers can vary with pointing direction.

Data format	Event size (bytes)	Rel. timing
Raw	1 μs	24
A1	10 μs	9
A2	10 μs	7
B1	10 μs	6
B2	0.4 ms	6
D1	10 μs	6
I	16 μs	2

Table 6.1: Timing accuracy relative to satellite clock, event size and average allowed count rate for a typical observation with the 7 different data formats. Note that the count rates are only rough guides and certainly not "hard limits".

In Table (6.1) is given the size of a each detected event for the different data formats. The allowed "average" count rate for each data format can by estimated by assuming a constant count rate between two ground contacts (taken to be 24 hours apart) and during this time span filling up the on–board memory capacity that is not being occupied by background counts. However, count rates derived this way should thus be taken with much care since significantly higher count rates can be accomodated for exposures significantly shorter than 10^5 s.

Generally, the RAW format retaining the most information for each event is preferred, but for bright sources other formats must be chosen. Going from format A2 to A1, information on the charge distribution between the read–out nodes (wire grid and micro strips) is not retained. The formats B1, B2 and I differ in relative timing accuracy, but retain otherwise the same information as the A1 format. The D1 format gives no position information, but records only the energy and the relative time. In the appendix "LEPC/HEPC data formats" details on the data formats are given.

OCS observations

The relatively low through–put of the OCS and the upper limit on the exposure time allows only studies of bright sources. Since the excellent spectral resolution of the OCS enables studies of X–ray emission lines to an accuracy orders of magnitudes better than achieved until now, it is important to select targets with reasonably well understood lines. This is even more important since only a limited energy range can be scanned because of the long required exposure time for the OCS. Hence targets showing lines with widths <1 eV are intrinsically the best candidates for OCS observations. Many targets are expected to show a welth of narrow lines when studied with a spectral resolution at the eV–level. Since the OCS response is fairly good over a large energy range the number of lines that in principle could be studied is enormous. But compared to the other XSPECT instruments, it is evident that the number of targets that can be studied with the OCS is fairly small. Hence the observing strategy for the OCS will obviously be to target the brightest possible sources of some interesting object classes and study a few of their lines in detail. When considering OCS observations for a given target, the following should be kept in mind:

- **LiF energy band.** The LiF crystals enable studies of the interesting Fe–K lines in the 6–7 keV range. The through–put for the LiF crystals is an order of magnitude larger than for the other three available OCS energy ranges.
- **Si energy band.** Lines from Si, S, Ar, Ca can be studied in this energy range.
- **RAP energy band.** The RAP energy range is ideally suited for studies of lines from low temperature plasmas, such as lines from Fe–L, Ne and O.
- **Multilayer energy band.** The multilayers enable spectroscopy in the energy range 0.2–0.285 keV, where many lines from low temperature plasmas are emitted. However, it must be kept in mind that the interstellar medium is heavily absorbing in this energy range. This absorption varies by a factor of five depending on the pointing direction.
- **Mapping several energy bands simultaneously.** Since the Si–crystals, RAP–crystals and the multilayers are on the same side of the OCS panel, scanning a range of Bragg angles results in three spectra. The energy resolution of LEPC/HEPC is used to determine which energy range a given photon “belongs” to. Hence the efficiency for this side of the OCS panel can in principle be tripled.
- **Limits on Bragg angle.** The shadowing of the OCS entrance doors and the vignetting of the XRT decreases the total through–put of OCS observations for certain Bragg angles. Settling upon a given minimum response, the limits for the Bragg angles can be derived from Fig.(5.4).
- **How to obtain a spectrum.** For scanning an energy range of a target, the following must be specified: Pointing direction, start Bragg angle, step size of Bragg angle, number of Bragg angle steps and exposure time for each step. When reaching one of the limiting Bragg angles from above, the satellite must be re–oriented slightly in order to continue the scan. For the new pointing direction, the new start Bragg angle must be specified and so on.

In the near future, spectra obtained with the OCS can be simulated with UM_TOOL, see the chapter “Simulating observations”.

Simulating observations

Introduction

This chapter is mainly intended to allow the proposer to assess the feasibility of proposed observations.

Estimating observing window

The viewing constraints are described in Chapter I. The software JMAN can be used to determine areas of the sky visible for a given time interval, or dates that a given target position can be observed. JMAN can be obtained via the WWW (**http://hea-www.harvard.edu/SXG/jman_sxg.html**) or via anonymous ftp (**ftp://sdcjx2.bnsc.rl.ac.uk/pub/jman/**).

Estimating count rates with PIMMS

Source count rates in LEPC/HEPC can be estimated using HEASARC's multi-mission simulator PIMMS. It is assumed that a spectral model and either an absolute flux or a count rate in another instrument are known. The following dialog illustrates the use of PIMMS to estimate the LEPC/HEPC rate for a source with a 7 keV thermal bremsstrahlung spectrum, interstellar absorption of 2.9×10^{20} cm^{-2}, and an ASCA SIS rate of 0.007 c s^{-1}. It should be noticed however that the above described XSPEC program gives more precise estimate of count rates, since the redshift of the sources is also included. In addition, XPSEC also provides the simulated spectrum of the source.

```
*** PIMMS version 2.3 ***
    1996 Jun 03 release
    (this version does not simulate images)
    Reading mission directory, please wait
* Current model is BREMSSTRAHLUNG, kT=  10.0000 keV; NH =  1.000E+21
   <--- Use 'MODEL' command to change
* By default, input rate is taken to be
 Flux (  2.000- 10.000 keV) in ergs/cm/cm/s
   <--- Use 'FROM' command to change the default
* Simulation product will be
 Count rate in ASCA SIS
   <--- Use 'INSTRUMENT' command to switch to another instrument
PIMMS > model brem 7.0 2.9e20
PIMMS > instrument sxg lepc
```

```
PIMMS > from asca sis
PIMMS > go 0.007
* For thermal Bremsstrahlung model with kT=  7.0000 keV; NH =  2.900E+20
  and  7.000E-03 cps in ASCA SIS
  (Model normalization =  3.014E-05)
* PIMMS predicts  7.420E-02 cps with SXG LEPC
PIMMS > instrument sxg hepc
PIMMS > go 0.007
* For thermal Bremsstrahlung model with kT=  7.0000 keV; NH =  2.900E+20
  and  7.000E-03 cps in ASCA SIS
  (Model normalization =  3.014E-05)
* PIMMS predicts  3.991E-02 cps with SXG HEPC
```

PIMMS may be obtained from the **/software/tools** directory in the anonymous ftp node **ftp://legacy.gsfc.nasa.gov**.

Simulating LEPC/HEPC spectra with XSPEC

Background

The total non–X–ray background is estimated to be $\sim 10^{-3}$ counts cm^{-2} s^{-1} keV^{-1} for either HEPC or LEPC. In a $3'$ diameter circle ($\sim$ 7 mm for a 8 m focal length), this corresponds to a rate of $\sim 9 \times 10^{-3}$ counts s^{-1} for HEPC (2 – 25 keV) and $\sim 3 \times 10^{-3}$ counts s^{-1} for LEPC (0.2 – 8 keV).

The diffuse X–ray background in HEPC & LEPC may be estimated using the effective area shown in Fig. (4.5) and a model XRB spectrum. In LEPC, we estimate the background by using spectral observations of Rocchia et al. (1984) for the soft X–ray background, and the ASCA spectrum of Gendreau et al. (1994) above 1 keV. For HEPC, we use the HEAO-1 spectrum of Boldt (1987). We find a value of ~ 3.4 counts s^{-1} deg^{-2} for LEPC and ~ 1.2 counts s^{-1} deg^{-2} for HEPC. In a $3'$ diameter circle, these correspond to rates of $\sim 6.7 \times 10^{-3}$ counts s^{-1} for LEPC and $\sim 2.3 \times 10^{-3}$ counts s^{-1} for HEPC. Readers should be aware, however, that the soft component of the XRB is dominated by galactic contributions and can vary with viewing direction by as much as a factor of 5.

The simulated background spectra including the instrumental, the galactic as well as the extragalactic background are represented in Fig. (7.1) and (7.2). The corresponding fits files lepc_tot_b.fak and hepc_tot_b.fak may be obtained from the directory **/usr/local/ftp/pub/srg/** in the anonymous ftp node **dsri.dk**.

An example of a simulation

HEPC/LEPC spectra can be simulated with the HEASARC XSPEC program. In the Chapter 2 of the XSPEC package User's Guide, there is a detailed explanation of how to obtain the observed spectrum for a given observation. The definitions contained within paragraph 2.3.1 are particularly usefull for the above described simulation.

The following dialog illustrates the simulation of the spectrum of the same cluster as the one for which counts have been estimated using PIMMS. The cluster is placed at a redshift $z = 0.65$ and the normalization has been scaled in order to give the flux observed by ROSAT (9×10^{-14} ergs/cm/cm/s in the energy range 0.5 – 2 keV).

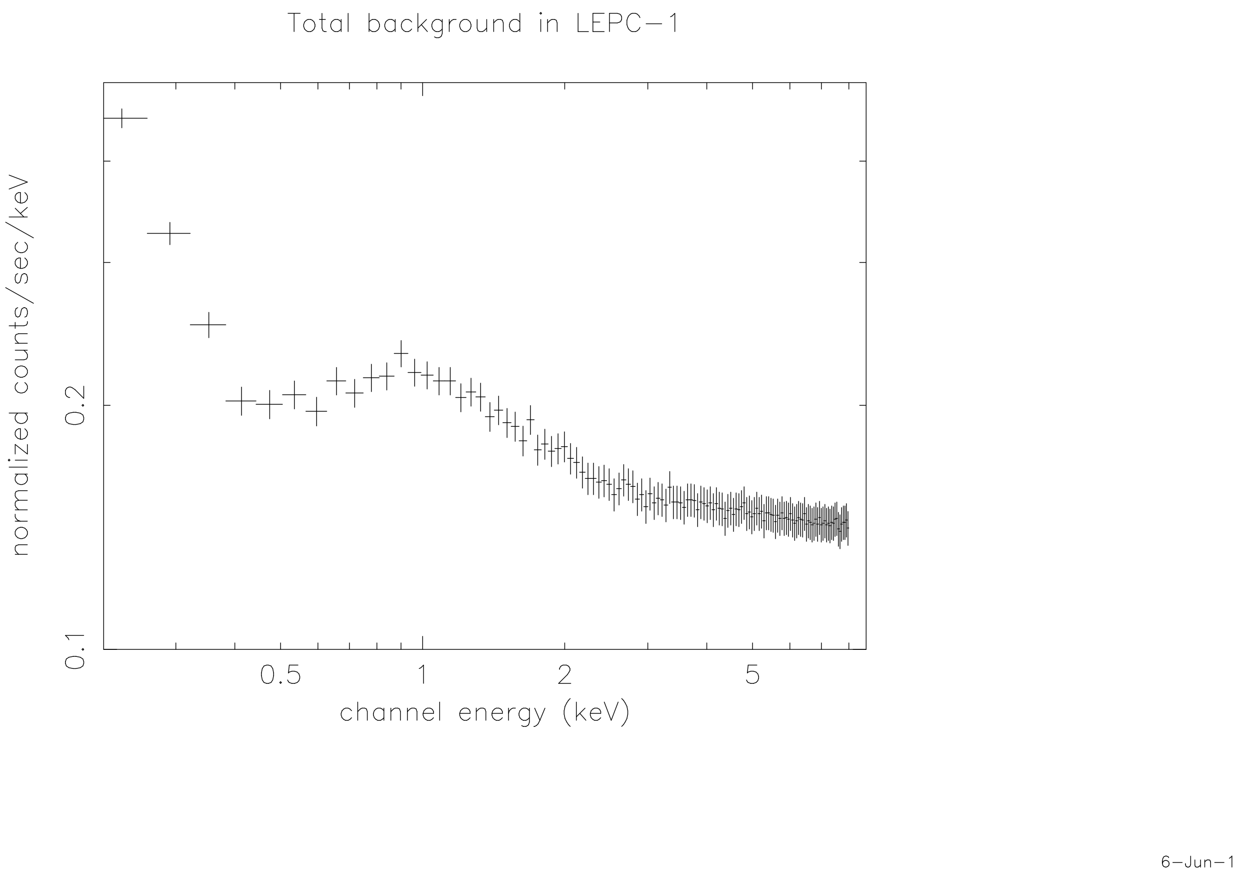

Figure 7.1: Simulated total background in LEPC-1, including the instrumental, the galactic and the extragalactic background

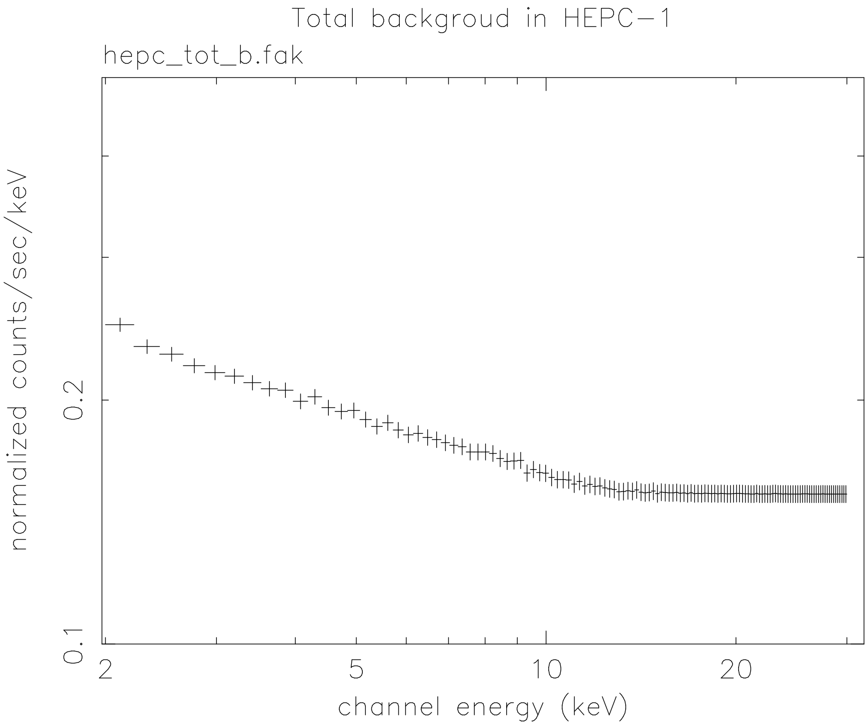

Figure 7.2: Simulated total background in HEPC-1, including the instrumental, the galactic and the extragalactic background

First we define a model on which we base the simulation. We choose an absorbed Raymond–Smith model with the above mentioned parameters and an abundance of 0.35 solar. We have left the normalization to its default value of unity, but it will be adjusted later.

```
              XSPEC 9.00 15:41:51  1-Jun-97
 XSPEC> mo wa ray
 mo = wabs[1] (raymond[2])
Input parameter value, delta, min, bot, top, and max values for ...
Mod parameter  1 of component  1 wabs     nH 10^22
   1.000      1.0000E-03      0.          0.      1.0000E+05  1.0000E+06
0.029
Mod parameter  2 of component  2 raymond  kT(keV)
   1.000      1.0000E-02  8.0000E-03  8.0000E-03   64.00       64.00
7.0
Mod parameter  3 of component  2 raymond  Abundanc
   1.000     -1.0000E-03      0.          0.       5.000       5.000
0.35
Mod parameter  4 of component  2 raymond  Redshift
      0.     -1.0000E-03      0.          0.       2.000       2.000
0.65
Mod parameter  5 of component  2 raymond  norm
   1.000      1.0000E-02      0.          0.      1.0000E+24  1.0000E+24

 ---------------------------------------------------------------------------
 ---------------------------------------------------------------------------
 mo = wabs[1] (raymond[2])
 Model Fit Model   Component     Parameter   Value
 par   par comp
   1    1    1       wabs        nH 10^22  2.900000E-02 +/-      0.
   2    2    2       raymond     kT(keV)    7.00000     +/-      0.
   3    3    2       raymond     Abundanc  0.350000     frozen
   4    4    2       raymond     Redshift  0.650000     frozen
   5    5    2       raymond     norm       1.00000     +/-      0.
 ---------------------------------------------------------------------------
 ---------------------------------------------------------------------------
   3 variable fit parameters
```

In order to derive the correct normalization, we first determine by using the commands `dummy` and `flux`, the flux of the model with the normalization of unity. Then we work out the new normalization and reset it with the command `newpar`.

```
XSPEC> dummy 0.5 2
XSPEC> flux 0.5 2
Model flux 0.1492     photons (2.4393E-10 ergs)cm**-2 s**-1 (  0.500-  2.000)
XSPEC> newpar 5 3.689e-04
   3 variable fit parameters
```

Here, we have changed the value of the normalization (the fifth parameter) from 1 to $9 \times 10^{-14}/2.4393 \times 10^{-10} = 3.689 \times 10^{-4}$ to give the flux observed by ROSAT.

We now check that the normalization is correct!

```
XSPEC> flux
Model flux 5.5036E-05 photons (8.9984E-14 ergs)cm**-2 s**-1 (  0.500-  2.000)
```

The simulation is initiated with the command fakeit. Since the argument none is given, the user is prompted for the name of the response matrix (if no argument is given, the current response is used). There will be no background included in these simulations.

```
XSPEC> fakeit none
 For fake data, file #  1 needs response file: hepc.rmf
             ... and ancillary response file : srg.arf
```

There then follows a series of prompts asking the user to specify whether he or she wants counting statistics (yes!), the name of the fake data file (the default name hepc.fak is left in our example), T (the integration time), A, Bkg (the background scale) and cornorm. In creating the first fake file, these last four parameters are left at their default values. In practice, A and cornorm can always be left at their default values.

```
Use counting statistics in creating fake data? (y)
 Input optional fake file prefix (max 12 chars):
Override default values for file #    1
 Fake data filename (hepc.fak):
 T, A, Bkg, cornorm ( 1.0000 , 1.0000 , 1.0000 , 0. ):
Net count rate (cts/s) for file   1      0.    +/-   11.31
Chi-Squared =     6.6896E-06 using   128 PHA bins.
Reduced chi-squared =     5.3517E-08
```

We then modify the keyword BACKGROUND in the fits file hepc.fak by using the command back. The fits file hepc_tot_b.fak will now be automatically included in the following simulations.

```
XSPEC> back hepc_tot_b.fak
Net count rate (cts/s) for file   1  -4.592    +/-   11.31
Chi-Squared =     0.1681     using   128 PHA bins.
Reduced chi-squared =     1.3449E-03
```

Now, the simulation is initiated with the command fakeit none. The current responses are then used.

```
XSPEC> fakeit
Use counting statistics in creating fake data? (y)
 Input optional fake file prefix (max 12 chars):
Override default values for file #    1
 Fake data filename (hepc.fak):
```

Now we ask for an integration time of 50000 seconds and renormalize the background to the area where the cluster detection is optimal, ie a $3'$ diameter region. Since the background has been computed for the full size of the detector, Bkg should be equal to $(1.5'/30')^2 = 2.5 \times 10^{-3}$.

```
 T, A, Bkg, cornorm ( 1.0000 , 1.0000 , 1.0000 , 0. ): 50000.0,1.0,2.5e-03,1.0
hepc.fak exists, reuse it ? y
Net count rate (cts/s) for file   1  1.0880E-02+/-  6.6916E-04( 48.7% total)
Chi-Squared =      172.8     using   128 PHA bins.
Reduced chi-squared =      1.383
```

XSPEC gives a value of $\sim 10^{-2}$ counts/s (notice that it is different from the one given by PIMMS) and the simulated data are contained within the fits file hepc.fak. The data can be plotted by the command `iplot`. The result is shown in Fig. (7.3)

The XSPEC package can be obtained from the **software/xanadu** directory in the anonymous ftp node **legacy.gsfc.nasa.gov**. The required and updated response matrices lepc.rmf and hepc.rmf and the effective area srg.rmf may be obtained from the directory **pub/srg/Curr..** in the anonymous ftp node **ftp.dsri.dk**.

Simulating LEPC/HEPC, SIXA and OCS spectra with UM_TOOL

The package UM_TOOL developed by Niels Jørgen Westergaard, DSRI, can be used for simulating spectra, count rates and exposure times for a given target. The count estimates are based on simple integrals between energy limits disregarding the finite detector energy resolution. All efficiencies are for on–axis sources. UM_TOOL is written in IDL and can be obtained at the DSRI SRG ftp area. Fig. (7.4) is an out–print of the UM_TOOL user interface window.

UM_TOOL is an IDL procedure where an optional parameter can be given, i.e.:

```
..IDL> um_tool
```

or

```
..IDL> um_tool,'um_tool_spec000.dat'
```

where the optional parameter is a file (in this example a spectral output file from the previous run of UM_TOOL). It must contain a definition of all the initial parameters.

Two widgets will be displayed on the screen, the bigger one is the actual interface (see Fig. (7.4)) and the smaller one is for display of results of the calculation.

In the following, the interface widget will be explained from top to bottom.

1. **Calculate the number of counts between these energies.**
   There are three windows. The two leftmost show the lower and upper energy limit (in keV) for the integration of the counts. The rightmost window is the center energy of the OCS (Objective Crystal Spectrometer) interval. This energy will be used for calculating OCS countrates.

2. **Energy band for source strength indication.**
   The source strength of a cosmic X-ray source is very often given as an energy flux (erg/cm^2/s) in a specified energy interval. This interval can be defined in the two windows.

3. **Source strength** and **Constant**.
   A constant to be multiplied on the spectral form is an alternative way of specifying the source intensity. The two "Active" buttons to the right defines which intensity specification is used.

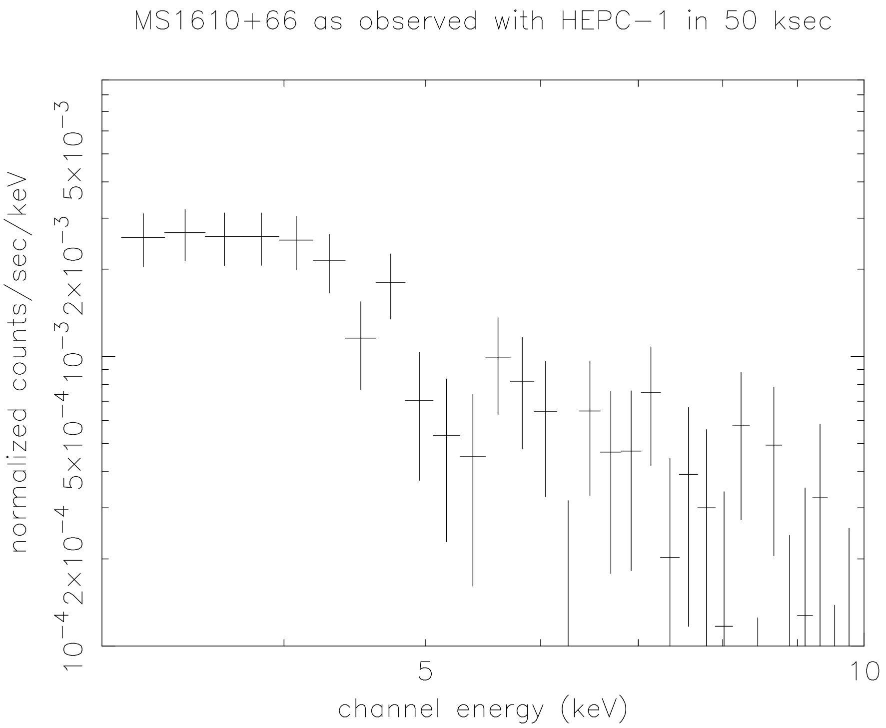

Figure 7.3: Simulated spectrum of a 7 keV cluster at z=0.65. The 0.5 –2 keV flux is 9×10^{-14} ergs/cm/cm/s and the expected count rate in HEPC is $\sim 10^{-2}$ cts/s.

4. **Select the spectrum.**
   This section consists of 3 rows and 7 columns. The first row is only used for labels. Row number 2 specifies the first contribution to the spectrum and row number 3 specifies the second contribution.
   Weight: A factor multiplied on the spectrum - can be zero if only one component is needed.
   Type: The currently available spectral types are: PL (power law), TB (thermal bremsstrahlung), MK (Mewe-Kaastra thin plasma), and TF (table file). When a table file is given the name of the file must be entered in the 'Table file' box.
   NH: The absorption column in equivalent H (cm^{-2})
   Table_file: Name of two-column ASCII file with photon spectrum. The first column should be the energy in keV and the second one the spectrum. Extra comment lines are allowed provided that they do not begin with $+-0.012345678$ or 9. Notice, that the interstellar absorption will be applied to a table file spectrum. Therefore the spectrum should be defined "at the source" or the "NH" value set to zero.
   Temp (keV): The plasma electron temperature kT – only for spectral models "TB" and "MK".
   Alpha: The power-law spectral photon index ($F = kE^{-\alpha}$) – only for spectral type "PL".
   Abundance: Metal abundance relative to solar – only for spectral type "MK".

5. **Observation time**: The exposure time has to be given in seconds. For OCS calculation this is the time per Bragg angle. A count spectrum plot for LEPC/HEPC/SIXA is calculated for the exposure time, but for OCS the time that must be exposed is the "Observation time" times the number of bins.

6. **Number of sigmas.**
   The Number of Sigmas (NOS) is the level of detection. The expression used is: $N_s(min) = NOS \times \sqrt{4 + N_b}$ or $NOS = N_s/\sqrt{4 + N_b}$ where N_s is the number of source counts, $N_s(min)$ the minimum number of source counts for a detection, and N_b is the number of background counts.

7. **Redshift z.**
   Not implemented.

8. **Detector selection row.**
   When selecting a detector the plotting range is defined. For OCS the range is defined around the "OCS Energy" (upper right corner) in a limited interval. If the "OCS Energy" is outside the useful interval for the crystal of choice another value is proposed.

9. **Action rows.**
   Calculate: Initiates a calculation of the parameters in the result display widget. With an OCS choice the results are for a point source and a single setting of the OCS panel. The results of the calculations are dumped to the log file:

   ```
   um_tool.log
   ```

in the directory from where you have started UM_TOOL.

Plot photon spectrum: Plots the photon spectrum including the interstellar absorption, in units of photons/cm^2/s/keV in the plot window.

Plot obs. spect/chan: Plots the number of source counts per channel for the specified instrument and for the observation time given. The channel width is the FWHM of the detector (rocking curve width for OCS). The error bars indicate $\pm\sqrt{\text{counts including background}}$.

Plot obs. spect/keV: Same as above but divided with the channel width.

DONE: Selfexplanatory.

Hardcopy: The hardcopy of the latest plot is directed to the printer with the UNIX command:

```
lpr um_tool_last_plot.ps
```

so it is printed on the default printer.

Save spectrum: The spectrum for the latest plot, regardless of type, is saved in a file named: um_tool_specnnn.dat in ASCII format. "nnn" is a serial number that begins with 000 and is updated for each saving. Notice, that each run of UM_TOOL will overwrite the saved files from previous runs. The data in the files can be read into IDL using the procedure "rstab" supplied with the UM_TOOL package. All the parameter settings are saved as well and can be used as default settings when UM_TOOL is started by giving the filename as parameter.

For more details, suggestions and comments on UM_TOOL, please contact Niels Jørgen Westergaard (njw@dsri.dk).

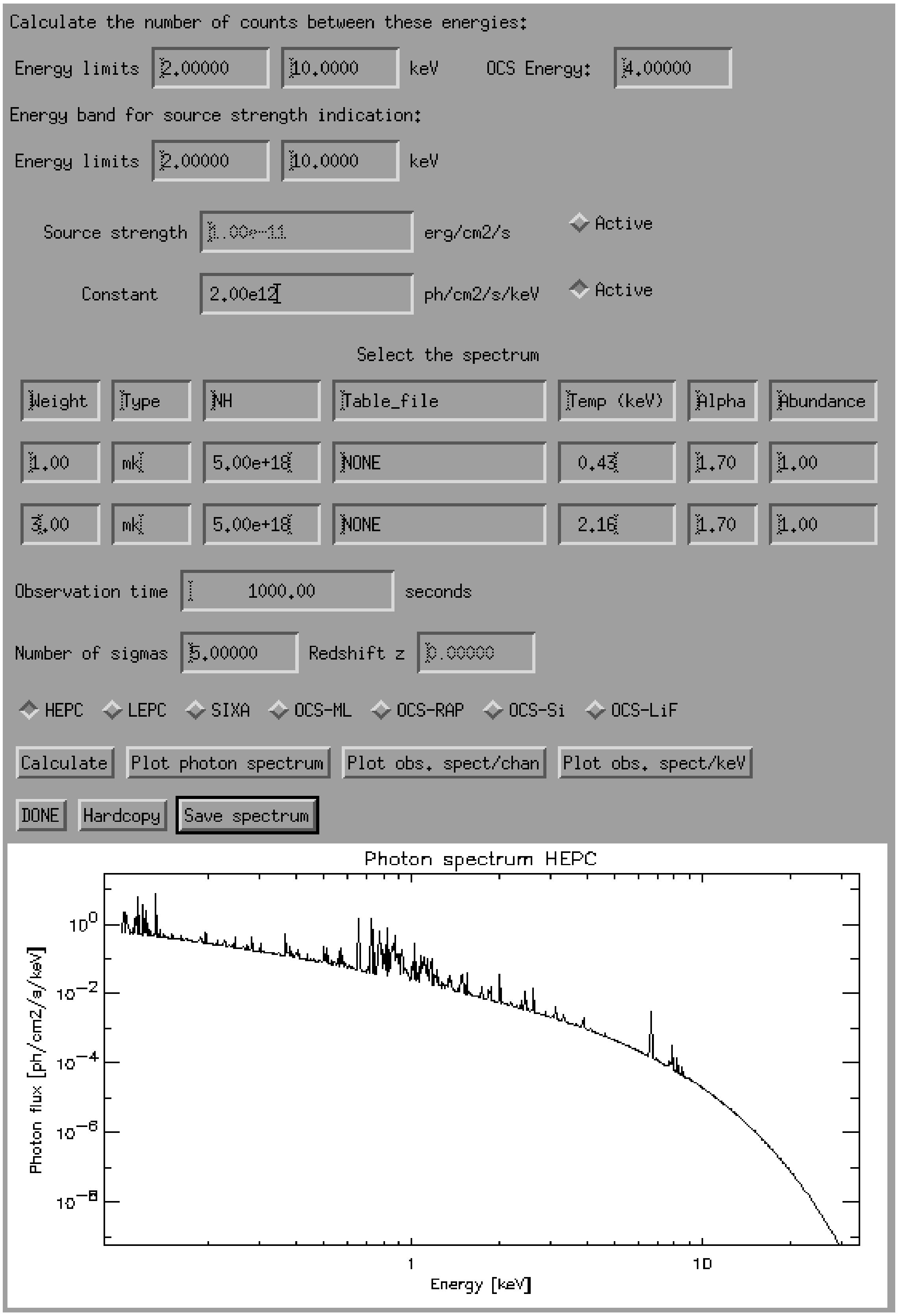

Figure 7.4: UM_TOOL user interface window.

List of contact persons

Below is a list of the key persons to contact and their areas of speciality.

Topic:	**Name:**	**e–mail**
XSPECT help desk		xspect-help@dsri.dk
Mirror system	Finn E. Christensen	finn@dsri.dk
HEPC/LEPC	Carl Budtz–Jørgensen	cbj@dsri.dk
	Mattias Møhl Madsen	mmm@dsri.dk
OCS	Finn E. Christensen	finn@dsri.dk
SIXA	Osmi Vilhu	osmi.vilhu@helsinki.fi
Calibration files	Niels Jørgen Westergaard	njw@dsri.dk
UM_TOOL	Niels Jørgen Westergaard	njw@dsri.dk
Proposal handling	Allan Hornstrup	allan@dsri.dk
Onboard software	Mattias Møhl Madsen	mmm@dsri.dk
XSPECT Observer's Handbook	Kristian Pedersen	kristian@dsri.dk
	Jamila Oukbir	jamila@dsri.dk

Other sources of information

DSRI SRG home–page	http://www.dsri.dk/srg/srg.html
XSPECT Observer's Handbook	http://www.dsri.dk/srg/userman.ps
XSPECT calibration files	ftp://ftp.dsri.dk/pub/srg/Curr.../
SRG mission operations report	http://www.dsri.dk/srg/tic/mor/mor.html
SRG in–flight calibration plan	http://www.dsri.dk/srg/if-cal/
JMAN program	http://hea-www.harvard.edu/SXG/jman_sxg.html
XSPEC package	http://legacy.gsfc.nasa.gov/docs/xanadu/xspec/u_manual.html
JET-X home–page	http://sdcjx2.bnsc.rl.ac.uk/
SIXA home–page	http://gstar.helsinki.fi/projects/sixa/sixa.html
TAUVEX home–page	http://www.tau.ac.il/ benny1/TAUVEX/welcome.html
IKI SRG home–page	http://hea.iki.rssi.ru/SXG/SXG–home.html
US SRG Coordination Facility	http://hea–www.harvard.edu/SXG/sxg.shtml
MART–LIME home–page	http://lheawww.gsfc.nasa.gov/docs/cai/coded_mart.html
MOXE home–page	http://nis–www.lanl.gov/nis–projects/moxe/
FUVITA home–page	http://www1.psi.ch/www_lap_hn/ASTR_FUV.HTML
ASCA US home–page	http://heasarc.gsfc.nasa.gov/docs/asca/ascagof.html
BeppoSax home–page	http://titan.ias.fra.cnr.it/ias-home/sax/sax_main.html
ROSAT All Sky Survey Bright Source Catalogue	http://www.rosat.mpe-garching.mpg.de/survey/rass-bsc/cat.html
XMM UK home–page	http://www.star.le.ac.uk/xmm/xmm_overview.html
AXAF home–page	http://hea-www.harvard.edu/asc/axaf-welcome.html

List of accronyms

CXRB	Cosmic X–Ray Background
DSRI	Danish Space Research Institute
FOV	Field Of View
GSFC	Goddard Space Flight Center
HEPC	High Energy Proportional Counter
HPD	Half Power Diameter
IKI	Russian Space Research Institute
LEPC	Low Energy Proportional Counter
OCS	Objective Crystal Spectrometer
PSF	Point Spread Function
SIXA	Silicon X–ray Array
SODART	SOvjet–DAnish Røntgen Telescope
SRG	Spectrum–Røntgen–Gamma
TOO	Target of Opportunity Observation
XRT	X–Ray Telescope
XSPEC	X–ray SPECtral fitting package
XSPECT	X–ray SPECtral and Timing mission concept

References

Boldt, E., 1987, *Physics Reports* **146**, 215.

Budtz–Jørgensen, C., Bahnsen, A., M., M., Olesen, C., Jonasson, P., & Schnopper, H., 1990, *SPIE* **1344**, 91.

Budtz–Jørgensen, C., Bahnsen, A., Møhl Madsen, M., Olesen, C., Jonasson, P., & Schnopper, H., 1992, *SPIE* 1743.

Budtz–Jørgensen, C., Bahnsen, A., Møhl Madsen, M., Olesen, C., Jonasson, P., & Schnopper, H., 1994a, *Nuclear Instruments & Methods in Physics Research A* **348**, 496.

Budtz–Jørgensen, C., Bahnsen, A., Møhl Madsen, M., Olesen, C., Jonasson, P., & Schnopper, H., 1994b, *SPIE* **2279**, 517.

Christensen, F., Madsen, B., Hornstrup, A., Abdali, S., Frederiksen, P., Westergaard, N., Polny, J., Budtz–Jørgensen, C., & Jonasson, P., 1997, *SPIE*.

Christensen, F., Westergaard, N., Rasmussen, I., Schnopper, H., Wiebicke, H.-J., Halm, I., Geppert, U., & Borozdin, K., 1994, *SPIE* **2279**, 511.

Condon, J., 1974, *Ap.J.* **188**, 279.

Gendreau, K., Mushotzky, R., Fabian, A., et al. 1994, *NEW HORIZON OF X–RAY ASTRONOMY – first results from ASCA* – p. 365.

Hacking, P. & Houck, J., 1987, *Ap.J.Suppl.* **63**, 311.

Rocchia, R., Arnaud, M., Blondel, C., Cheron, J., Rothenflug, R., Schnopper, H., & Delvaille, J., 1984, *A&A* **130**, 53.

Schnopper, H., 1994, *SPIE* **2279**, 412.

Schnopper, H. & Byrnak, B., 1987, *App. Opt.* **26**, 2871.

Vilhu, O., Huovelin, J., Tikkanen, T., Hakala, P., Muhli, P., Kämäräinen, V., Sipilä, H., Taylor, I., Pohjonen, J., Päivike, H., Toivanen, J., Sunyaev, R., Kuznetsov, A., & Abrosimov, A., 1994, *SPIE* **2279**, 532.

Wiebicke, H.-J., Halm, I., Christensen, F., Westergaard, N., & Abdali, S., 1997, *SPIE* 3113.

Appendix

LEPC/HEPC data formats

Events detected by LEPC/HEPC can be recorded in 7 pre–defined data formats. Below these modes are described, in order of decreasing degree of information retained for each event, and the information recorded for each mode is and the size per event is listed.

RAW Signal from each read–out node of micro strip plate.
Signal from each read–out node of wire grid.
Signal from veto area.
32 bit time from satellite clock in units of μs.
Size: 24 bytes.

A2 Derived position on micro strip plate.
Derived position on wire grid.
Signal from veto area.
Derived energy.
Pulse rise time.
16 bit time difference relative to previous event in units of 10 μs.
Size: 9 bytes.

A1 Derived position on micro strip plate.
Charge ratio on micro strip plate.
Derived position on wire grid.
Charge ratio on wire grid.
Signal from veto area.
Derived energy.
Pulse rise time.
16 bit time difference relative to previous event in units of 10 μs.
Size: 7 bytes.

B1 Derived position on micro strip plate.

Derived position on wire grid.
Signal from veto area.
Derived energy.
Pulse rise time.
8 bit time difference relative to previous event in units of 10 μs.
Size: 6 bytes.

B2 Derived position on micro strip plate.
Derived position on wire grid.
Signal from veto area.
Derived energy.
Pulse rise time.
8 bit time difference relative to previous event in units of 0.4 ms.
Size: 6 bytes.

I Derived position on micro strip plate.
Derived position on wire grid.
Derived energy.
Pulse rise time.
Signal from veto area.
16 bit time difference relative to previous event in units of 16 μs.
Size: 6 bytes.

D1 Derived energy.
8 bit time difference relative to previous event in units of 10 μs.
Size: 2 bytes.